NACA

RESEARCH MEMORANDUM

THE USE OF THE ROLLED-UP VORTEX CONCEPT FOR PREDICTING WING-TAIL INTERFERENCE AND COMPARISON WITH EXPERIMENT AT MACH NUMBER OF 1.62 FOR A SERIES OF MISSILE CONFIGURATIONS HAVING TANDEM CRUCIFORM LIFTING SURFACES

By Carl E. Grigsby

Langley Aeronautical Laboratory
Langley Field, Va.

NATIONAL ADVISORY COMMITTEE
FOR AERONAUTICS

WASHINGTON

September 24, 1952

Classification cancelled (or changed to Unclassified)

By authority of NASA Tech Pub Announcement #103

(NOTICE OF CHANGE)

By ..... 28 Aug 56

NK

GRADE OF OFFICER MAKING CHANGE

5 Apr. 61

DATE

[redacted]

NATIONAL ADVISORY COMMITTEE FOR AERONAUTICS

RESEARCH MEMORANDUM

THE USE OF THE ROLLED-UP VORTEX CONCEPT FOR PREDICTING WING-TAIL INTERFERENCE AND COMPARISON WITH EXPERIMENT AT MACH NUMBER OF 1.62 FOR A SERIES OF MISSILE CONFIGURATIONS HAVING TANDEM CRUCIFORM LIFTING SURFACES

By Carl E. Grigsby

SUMMARY

The method for predicting wing-tail interference whereby the trailing vortex system behind lifting wings is replaced by fully rolled-up vortices has been applied to the calculation of tail efficiency parameters, lift characteristics, and center-of-pressure locations for a series of generalized missile configurations. The calculations have been carried out with assumed and experimental vortex locations, and comparisons made with experimental data.

The measured spanwise locations of the vortices for the inline case were found to be in good agreement with the asymptotic values computed from the center of gravity of the vorticity using the method of Lagerstrom and Graham. For the interdigitated configurations the measured spanwise locations were in only fair agreement with the asymptotic locations computed for the inline case. The vertical displacement of the vortices with angle of attack for both inline and interdigitated configurations was small.

The method utilizing the rolled-up vortex concept was shown to give good results in the prediction of tail efficiency variations with angle of attack for inline configurations. Not as good correlation with experiment was shown for the interdigitated configurations. Complete configuration lift-curve slopes and center-of-pressure locations, obtained using tail efficiency calculations together with the characteristics of the components obtained from available theoretical methods, showed excellent correlation with experimental results.

[redacted]

[redacted]

INTRODUCTION

A rational approach to longitudinal stability and control problems must include a knowledge of the downwash field behind the forward lifting surfaces. Furthermore, the use of low-aspect-ratio lifting surfaces and cruciform configurations has forced a reexamination of the methods and assumptions used in the past to predict the downwash behavior behind lifting surfaces. Spreiter and Sacks (ref. 1) have investigated the rolling up of the trailing vortex sheet and its effect upon the downwash field behind plane wings. In the investigation of reference 1 the rates of rolling up of the trailing vortex sheets of wings of similar span loading were found to vary directly with lift coefficient and inversely with the aspect ratio. Thus, for low-aspect-ratio wings, such as might be used on missiles, the trailing vortices would be essentially rolled up within a short distance of the wing even at low lift coefficients. It appears, therefore, that for configurations having low-aspect-ratio lifting surfaces the assumption whereby the trailing vortex sheet is replaced by a single horseshoe vortex is in reasonable agreement with the physical picture.

Similar results for the plane-wing case have been found in the theoretical investigation of Lagerstrom and Graham (ref. 2) in which a simplified cross-flow treatment of the problem was utilized. In addition, this investigation has examined the motion of the vortices in the presence of an infinite circular cylinder or, for practical purposes, has extended the method to wing-body combinations. Under the assumptions of the simplified cross-flow treatment, the solution is the classical solution of two vortices in the presence of a circular cylinder in incompressible flow such as is given by Milne — Thomson (ref. 3).

Thus, for plane configurations where the vortex sheet may be assumed to be fully rolled-up, the downwash field behind the body-wing combination may be obtained. With the aid of theoretical methods which make use of reversibility concepts (refs. 4 and 5) and the superposition method of reference 6, the lift of the tail in the nonuniform downwash field may be determined and the longitudinal stability characteristics of a complete body-wing-tail configuration found.

The more complicated behavior of the vortex system behind cruciform wings has been investigated by Sacks in reference 7 and closed solutions obtained for the motions of four equal strength vortices behind cruciform wings. These solutions must be modified to account for the effects of the body upon the motions of the vortices, and for the unequal circulations of the upper and lower pairs of vortices. Solutions may be obtained with the use of numerical integration, but they become laborious. Simplifications are thus necessary if solutions may be easily obtained for these

configurations. Because of these considerations and the fact that in the development of the methods discussed above both slender-body and linear theory were used to determine decidedly nonlinear effects, it is obvious that experimental verification is necessary if these methods are to be used with any certainty. Comparisons with experiment have been made for an air-to-air missile at Mach number of 1.4 by Edwards (ref. 8), and for a number of missile configurations at Mach numbers of 1.62 and 1.93 by Rainey (ref. 9). These results have shown reasonable agreement between experimental and calculated longitudinal stability characteristics.

The purpose of the present investigation is to extend the calculations of wing-tail interference using fully rolled-up vortices to a series of generalized missile configurations. The results of tests of these configurations made in the Langley 9-inch supersonic tunnel at a Mach number of 1.62 have been reported in reference 10. These configurations, having simple lifting surfaces, are more amenable to theoretical analysis and allow systematic comparisons to be made for a number of geometric variables. In this way, it is hoped that some insight may be gained concerning the accuracy and range of applicability of the method using fully rolled-up vortices for predicting wing-tail interference.

SYMBOLS

a	body radius
x,y,z	cartesian coordinates (when used in calculations of wing-tail interference, origin is at center of body at wing trailing-edge location, see fig. 1)
S	wing area
α	angle of attack
U	stream velocity
$V = U\alpha$	
v	velocity at any point due to circulation of vortex
C_L	lift coefficient
c.p.	center of pressure; distance measured in body diameters from center of gravity

[redacted]

Γ_o circulation about root chord of wing

η_t tail efficiency parameter

B configuration of body

BT configuration of body and tails

BW configuration of body and wings

BWT configuration of body, wings, and tails

Subscripts:

1,2,...6 refers to a particular wing or tail plan form

F wing in forward location

R wing in rear location

i initial vortex location

∞ asymptotic vortex location

eq equivalent angle of attack or yaw when configuration is pitched and rolled

Superscripts:

0,45 angle between a plane through opposite tail panels and a plane through opposite wing panels. The angle is always less than 90^o, and its value appears as the superscript for W in the complete configuration designation.

THEORETICAL METHODS

Calculation of downwash field behind body-wing combination, inline case.- In the calculation of downwash behind a body-wing combination, it will be assumed that the vortex sheet discharged from the trailing edge of the wing panel may be considered fully rolled-up into a discrete vortex at the tail location. Thus, the total vorticity of the lifting wing panel is concentrated into a single line vortex whose strength and initial location are a function of the span load distribution of the wing panel. These functions and methods of analysis are now well-known, but they will be briefly summarized here together with the assumptions used in the present calculations.

The strength of the trailing vortex is known since it must be equal to the sum of all the vortices discharged from the wing or, in other words, the magnitude of the circulation around the wing in the plane of symmetry. Thus, for the present calculations, the strength of the trailing vortex Γ_o is related to the span loading of the wing panel by

$$\Gamma_o = \frac{U}{2}\left(c_l c\right)_{y=a} \tag{1}$$

where $\left(c_l c\right)_{y=a}$ is the value of span loading at the wing-body juncture. The span load distribution of each wing panel was determined by considering only the exposed wing panel and neglecting the effect of wing-body interference. As has been discussed in detail in references 1 and 2, the initial location of the trailing vortex was taken to be the center of gravity of the actual vortex sheet. This center-of-gravity location was found from the span loading by

$$y_{i_-} = \frac{C_L S}{\left(c_l c\right)_{y=a}} + a \tag{2}$$

Knowing the strength and initial location of the trailing vortex, the path of the vortex downstream must also be determined. Lagerstrom and Graham have made use of a simplified "cross-flow" treatment to determine the motion of two line vortices in the presence of a circular cylinder. The path of the vortices may be determined from the general equation of the motion of the vortices by numerical integration; however, the asymptotic spacing of the vortices which has been determined as a limit of the general equation is defined by the closed expression

$$2y_\infty - \frac{\Gamma_o}{2\pi V} \log_e 2y_\infty = B \tag{3}$$

where

$$B = 2y_i\left(1 - \frac{a^2}{{y_i}^2}\right) - \frac{\Gamma_o}{2\pi V} \log_e \frac{2y_i\left({y_i}^2 - a^2\right)}{{y_i}^2 + a^2}$$

[redacted]

This asymptotic spacing has been used for the inline configurations in the present calculations as the vortex spacing at the tail location. The values shown are independent of angle of attack although Γ_o which is proportional to angle of attack is directly involved in determining y_∞. The effect of varying Γ_o upon y_∞ is, however, small and has been neglected. The vertical displacement of the trailing vortex was determined from the approximate relation

$$z = -0.1\alpha(l \cos \alpha) \tag{4}$$

where l is the distance from the wing trailing edge to the leading edge of the tail. This equation was found to give a good approximation to the results of Lagerstrom and Graham. In the foregoing analysis image vortices are placed within the body so that the boundary condition of tangential flow at the body surface would be satisfied.

Once the strength and location of the trailing vortices at the tail are known, the downwash distribution can be easily determined since the velocity at any point resulting from the circulation of the vortex is

$$v = \frac{\Gamma_o}{2\pi r} \tag{5}$$

where r is the distance from the point considered to the vortex. Determining the vertical velocity or downwash velocity over the tail span is then simply a matter involving the geometry of the tail and the vortex locations. In this analysis changes in dynamic pressure at the tail are not considered.

Interdigitated case.- For the interdigitated case the determination of the strength of the trailing vortex is not as simple as for the inline case. Since each pair of wing panels is at an equivalent angle of attack and angle of yaw, the strength of the vortices may be found by considering the span loading of the exposed wing panels at a condition of yaw and pitch. If the wing plan form has small rolling moment due to yaw, then the span loading may be determined from the angle of attack in the plane of symmetry of the wing panels. This angle of attack is simply

$$\alpha_{eq} = \tan^{-1}(\tan \alpha \cos 45^\circ) \tag{6}$$

If, on the other hand, the rolling moment due to yaw is large, then the span loading may be calculated using existing linear theory results. This procedure has been applied by Edwards (ref. 8) to a configuration

having triangular wings of 60° leading-edge sweep. Excellent agreement was found between the calculated and experimental values of total lift on the individual wing panels. As would be expected from consideration of the pressure distribution over the wing panels, the lower or leading panels showed a considerable increase in lift with increasing angle of attack while the upper or trailing panels showed almost an equivalent loss in lift. In the calculations made here, consideration of the rolling moment due to yaw was made for the configurations having triangular wings (BW_5T_5 and BW_5T_4). For the configurations having zero leading-edge sweep, it was assumed that there was no significant rolling moment due to yaw. The results of Sacks (ref. 7) allow the path of four vortices to be determined where the four vortices are of equal strength. This method, when modified to include body effects, becomes laborious and was not attempted for these calculations. In view of the difficulty associated with determining the motion of the vortices, a gross assumption regarding their location was made, namely, that the vortices originated at the wing tips and had vertical displacement but no spanwise movement downstream of the wing. The vertical displacement was assumed to be equal to that for the inline case. Calculations made using this assumption were found to be in poor agreement with experiment and will be discussed later. Then, experimental measurements of the vortex locations at the tail were made and these results were also used in the calculation. These experimental measurements will be discussed in detail later.

Once the location and strength of the trailing vortices were known, the downwash distribution was determined in the same manner as that used for the inline case.

Calculation of tail efficiency parameter.- The tail efficiency parameter η_t has been found useful in analyzing the over-all wing downwash effects. The parameter is defined as the ratio of the lift of the tail in the presence of the body and wing to the lift of the tail in the presence of the body. Experimental breakdown force data may be reduced to give values of tail efficiency by use of the relation

$$\eta_t = \frac{C_{L_{BWT}} - C_{L_{BW}}}{C_{L_{BT}} - C_{L_B}}$$

Now, for calculative purposes this relation is expressed in the form

$$\eta_t = 1 - \frac{\left(\Delta C_{L_t}\right)_W}{\left(C_{L_t}\right)_B}$$

[redacted]

Both the tail lift increment due to the presence of the wing $\left(\Delta C_{L_t}\right)_W$ and the tail lift in the presence of the body $\left(C_{L_t}\right)_B$ can be determined using the downwash distributions obtained previously and existing theoretical methods. The principal difficulty lies in determining the lift of the tail in the nonuniform wing downwash and body upwash fields. Considerable theoretical information exists regarding the calculation of lift in a nonuniform stream. To summarize the present information, it may be said that, with the aid of reversed flow theorems, exact results within the limits of the linear theory may be simply obtained. In the present calculations the results of Alden and Schindel (ref. 4) have been used to obtain the lift of the tail in the presence of the calculated downwash field and in the presence of the upwash field due to the body. The flow field about the body was assumed to be the incompressible flow about an infinite cylinder. Body-tail interference effects other than the calculations of body upwash previously discussed were not considered.

RESULTS AND DISCUSSION

Experimental location of trailing vortices.- Representative schlieren pictures illustrating the vortex patterns for both inline and interdigitated configurations are shown in figure 2. These pictures also illustrate the pitot-tube technique used in the systematic surveys locating the trailing vortices. These surveys are an extension of the tests of reference 10, and the models and test conditions are the same as those reported therein. The pitot tube used in the surveys is shown in the schlieren pictures to the rear and above the model. The regions of concentrated vorticity appear in the schlieren pictures as regions of highest density change and in the pitot measurements as points of miminum dynamic pressure. The configurations investigated both by the systematic pitot-tube survey and by the theoretical calculations are shown in figure 3.

The results of the pitot-tube surveys are shown in figures 4 to 7 and 9 to 13 as the vertical and spanwise locations of the vortices as functions of angle of attack referred to the axes of figure 1. The vortices discharged from the body (see ref. 11) were also located in the surveys but are not presented since they were not included in the calculations. Shown on the curves for the inline configurations are the calculated vortex locations and the vertical location of the tail leading edge at each angle of attack. The curves for the interdigitated configurations contain the assumed vortex locations, the vertical location of the tail leading edge at each angle of attack, and, in addition, the calculated locations for the inline case which are shown for comparison.

The measured values of the spanwise locations of the vortices for the inline configurations (figs. 4, 6, 9, and 11) are generally in good agreement with the asymptotic values computed from the center of gravity of the vorticity using the method of Lagerstrom and Graham. The calculated locations for the rectangular wings (W_2 and W_3) are somewhat inboard of the experimental locations. For the reversed triangular wing configuration ($BW_{4F}{}^{0}T_4$ shown in fig. 9) good agreement with experiment was shown only if an elliptical wing loading was used although linear theory predicts triangular loading for this plan form. Good agreement was also shown for the inline cases for the vertical location of the vortices which was nearly a streamwise plane passing through the wing trailing edge.

The agreement between the assumed vortex locations and the measured locations (figs. 5, 7, 10, 12, and 13) was poor for the interdigitated configurations. This lack of agreement is as would be expected in view of the gross assumptions made for these configurations. When the asymptotic vortex locations calculated for the inline case are considered, considerably better correlation with experiment is shown, especially for the configurations having zero tip chord. The effect of the body which is to move the upper vortices inboard and the lower vortices outboard with increasing angle of attack is shown by the experimental spanwise locations. The motion of the lower vortices with angle of attack which have the largest influence on the downwash at the tail is, however, small for the aspect ratios and tail length considered here and the assumptions regarding the vortex motion discussed previously appear to be adequate for computational purposes.

Comparison of experimental and calculated values of tail efficiency.- A comparison of the experimental values of tail efficiency from reference 10 and the values calculated using assumed and measured vortex locations is given on the lower portion of figures 4 to 14. The shape of the calculated tail efficiency curves are as would be expected from downwash considerations, that is, the angle of minimum η_t is near 0° for the inline configurations, and for the interdigitated configurations occurs at an angle of attack which corresponds approximately to the angle at which the tail passes through the trailing vortices. If the inline configurations having rectangular wings and tails (figs. 4 and 6) for which the calculated vortex locations were slightly inboard of the measured locations are considered, the calculated η_t values are somewhat higher than the experimental values. In general the correlation may be considered good with the greatest discrepancy shown in the angle-of-attack range around 5° and of the order of 0.2. Agreement for the interdigitated cases (figs. 5, 7, and 8) is not as good as for the inline case although the shape of the tail efficiency curve was predicted with good accuracy, with the exception of the configurations having T_6 tail plan form (fig. 8).

[redacted]

The calculated tail efficiency values using an elliptical wing loading for the reversed triangular wing configurations are in fair agreement with experiment for the inline configuration as shown in figure 9. For the interdigitated case (fig. 10) the calculated values using experimental vortex location show good correlation with experiment. The quite different shapes of the two calculated tail efficiency curves for the interdigitated case are the result of the large difference between the assumed and measured vortex location which was discussed previously.

The calculated values for the inline case of the configurations having triangular wings ($BW_{5F}{}^{O}T_{5}$ and $BW_{5F}{}^{O}T_{4}$) are in good agreement with experiment as is shown on figures 11 and 14. For the interdigitated configurations (figs. 12, 13, and 14), however, it is evident that the calculated values do not give an accurate prediction of the shape of the tail efficiency curve and the angle of minimum η_t. The calculated angle of minimum η_t is displaced from the experimental by about 2° to 3°. Detail examination of schlieren pictures of these configurations yields some understanding regarding this lack of agreement. It appears that there are several regions of concentrated vorticity instead of the single fully rolled-up vortex assumed in the calculations. This observation is supported by evidence from unpublished data for several triangular wings of varying leading-edge sweep. From this data it was found that for wings having the leading edge near the Mach line, such as the W_5 plan form, the vorticity was concentrated into two vortices of nearly equal strength. If some of the vorticity is distributed inboard of the assumed location, the effect for interdigitated configurations will be to reduce the angle of minimum η_t as is illustrated in figures 12, 13, and 14. It would be expected that this inboard distribution of vorticity would have little effect on the angle of minimum η_t for inline configurations. Although the assumption of a single fully rolled-up vortex does not appear justified for the triangular-wing configurations, the maximum discrepancy between experimental and calculated values of η_t is about 0.30 shown for the wing rear configuration. It will be noted by comparison of figures 12 and 13 that the effect of moving the wing rearward in increasing the angle of minimum η_t was predicted by the calculations.

Thus, it appears from the comparisons made here that the calculative method will give quite good results in the prediction of tail efficiency variations with angle of attack for inline configurations. The calculative results for the interdigitated cases are not in as good agreement with experiment as the inline cases even when experimental vortex locations are used. Since the interdigitated configurations have higher downwash over the tails at angles of attack than do inline

configurations, it would be expected that any deviations at angle of attack from the linear theory span load distributions used in the calculations would be more serious for the interdigitated configurations. An example of the effect of angle of attack upon span load distribution may be seen in reference 12 where at $\alpha = 20^{\circ}$ the span loading for a triangular wing of 68.6° sweep is no longer elliptical, but is essentially triangular. There exists little experimental data concerning this effect especially for body-wing configurations and, consequently, linear-theory results must be utilized. The largest deviations between experiment and calculated values are shown for the interdigitated configurations where it is indicated that the total vorticity is not concentrated into a single vortex as is assumed.

Comparison of calculated and experimental lift coefficients and center-of-pressure locations.- The calculated tail efficiency values have been applied to the calculation of complete configuration lift coefficients, and center-of-pressure locations. In this way the usefulness of the calculative method in predicting these static longitudinal stability parameters may be determined. The results of the applications to the calculation of center-of-pressure locations are shown in figure 15, and a representative comparison of experimental and calculated lift coefficients is shown in figure 16. The experimental results for the complete configurations and their components were obtained from reference 10. The assumed center-of-gravity location of the models was 6.25 body diameters from the nose or 4.375 inches as is shown in figure 3. The individual components will be discussed first, and their combination to give the complete configurations will be discussed later.

The body-alone center-of-pressure results are presented in figure 15(a) and compared with the results of reference 11. Although there is considerable difference shown between the experimental and calculated values in the moderate angle-of-attack range, it has been found that these differences are not significant in the calculation of the complete configuration center of pressure.

The calculated values of center-of-pressure locations for the BW and BT configurations (shown in figs. 15(a) to 15(m)) were obtained using existing theoretical methods. The body contribution was determined from reference 11 as discussed above, and the wing plus interference was obtained from reference 13 assuming that the center of pressure of the exposed wing was unchanged by interference. The center of pressure of the lift on the body due to the wing was taken from the results of reference 14. The BT computations were identical to the BW except that the lift on the body due to the tail was neglected. The calculated values for the BW configurations are consistently rearward of the experimental locations by about 0.25 to 0.50 body diameter. This agreement is consistent with the comparisons given in reference 14 for a large number of configurations. The more forward location indicated by

[redacted]

experiment is believed to be the result of separation on the wing panels, and negative lifts on the afterbody. The BT correlation with experiment is somewhat better than the BW especially for the triangular and the reversed-triangular tail configurations. The forward location of the calculated values for the rectangular tail configurations may possibly be the result of neglecting the lift on the body due to the tail in the calculations.

The lift-curve slopes of the individual components discussed above were combined assuming no mutual interactions other than those discussed previously to give the complete configuration lift-curve slopes given in the following table:

Configuration	$(C_{L_\alpha})_{L\rightarrow 0}$	
	Experimental	Calculated
$BW_{2F}{}^{0}T_{2}$	0.3110	0.3199
$BW_{2F}{}^{45}T_{2}$	.4010	.3983
$BW_{3F}{}^{0}T_{2}$	.3080	.3191
$BW_{3F}{}^{45}T_{2}$	.4200	.4296
$BW_{2F}{}^{45}T_{6}$	.4450	.4452
$BW_{3F}{}^{45}T_{6}$	.4615	.4785
$BW_{4F}{}^{0}T_{4}$	.2210	.2371
$BW_{4F}{}^{45}T_{4}$	.2505	.2568
$BW_{5F}{}^{0}T_{5}$	.2050	.2034
$BW_{5F}{}^{45}T_{5}$	.2400	.2568
$BW_{5F}{}^{0}T_{4}$	.2305	.2371
$BW_{5F}{}^{45}T_{4}$	.2610	.2642
$BW_{5R}{}^{45}T_{5}$	.2385	.2548

The calculated lift-curve slopes were obtained for the inline configurations, using the vortex locations given by Lagerstrom and Graham, and for the interdigitated configurations, using the measured vortex locations.

Excellent correlation is shown between the experimental and calculated lift-curve slopes for both inline and interdigitated configurations. The comparison shown in figure 16 illustrates the correlation between experimental and calculated lift coefficients at varying angle of attack for representative configurations. Excellent correlation is shown in the low angle-of-attack range as was illustrated previously with some divergence between experiment and calculated lift coefficients shown at the higher angles. The correlation for the configurations not shown were within the limits illustrated in figure 16.

The center-of-pressure locations for the complete configurations are shown in figure 15. The variation of center-of-pressure location with angle of attack for this class of configurations is well-known, that is, the forward movement of center of pressure for the conditions in which highest downwash and, consequently, lowest tail lift is realized. These variations with angle of attack for both inline and interdigitated configurations are predicted with good accuracy by the calculations, and the correlation between experiment and calculated values is considered quite good. The average deviation of the calculated values from the experimental locations is about 0.2 body diameter with the greatest disagreement which was about 0.4 body diameter shown for the interdigitated cases of the triangular-wing configurations. For these configurations, it will be remembered that the vorticity was indicated to be concentrated into several vortices, not the single fully rolled-up vortex assumed in the calculations. The excellent agreement shown is somewhat fortuitous in view of the compensating effects of the more rearward location shown for the BW configurations, and the more forward location shown for the BT configurations. In view of the range of geometric variables covered in this comparison, it appears that the longitudinal stability characteristics of a missile configuration of the class considered here could be predicted with good accuracy. In fact, a design calculation in which available experimental data for the characteristics of the configuration components could be utilized should be in even better agreement with experimental results for the complete configuration than are the calculated results of this paper.

CONCLUSIONS

The method for predicting wing-tail interference whereby the trailing vortex system behind lifting wings is replaced by fully rolled-up vortices has been applied to a series of generalized missile configurations. The calculations have been carried out with assumed and experimental vortex locations, and comparison of the results with experimental results have indicated the following conclusions:

[redacted]

1. The measured spanwise locations of the trailing vortices as determined from the pitot-tube surveys were found, for the inline configurations, to be in good agreement with the asymptotic values computed from the center of gravity of the vorticity using the method of Lagerstrom and Graham. The vertical displacement of the vortices with angle of attack was shown to be small.

2. The measured spanwise locations of the vortices for the interdigitated configurations were in only fair agreement with the calculated locations which were obtained from the asymptotic values for the inline configurations. The vertical displacement of the vortices with angle of attack was small.

3. A comparison of experimental and calculated tail efficiency values has shown that the method utilizing the rolled-up vortex concept will give good results in the prediction of tail efficiency variations with angle of attack for inline configurations. Not as good correlation was shown for the interdigitated configurations.

4. Complete configuration lift-curve slopes at zero lift and center-of-pressure locations, obtained using the tail efficiency calculations together with the characteristics of the components as obtained from available theoretical methods, showed excellent correlation with experimental results. Some divergence between the experiment and calculated lift coefficients was shown at the higher angles of attack. In view of the results of the comparisons made herein, it appears that the static longitudinal stability characteristics of a missile configuration of the class considered in this report can be predicted with good accuracy.

Langley Aeronautical Laboratory,
National Advisory Committee for Aeronautics,
Langley Field, Va.

REFERENCES

1. Spreiter, John R., and Sacks, Alvin H.: The Rolling Up of the Trailing Vortex Sheet and Its Effect on the Downwash Behind Wings. Jour. Aero. Sci., vol. 18, no. 1, Jan. 1951, pp. 21-32, 72.

2. Lagerstrom, P. A., and Graham, M. E.: Aerodynamic Interference in Supersonic Missiles. Rep. No. SM-13743, Douglas Aircraft Co., Inc., July 1950.

3. Milne-Thomson, L. M.: Theoretical Hydrodynamics. Second ed. Macmillan and Co., Ltd., 1949.

4. Alden, Henry L., and Schindel, Leon H.: The Calculation of Wing Lift and Moments in Nonuniform Supersonic Flows. Guided Missiles Program, M.I.T. Meteor Rep. No. 53, May 1950.

5. Morikawa, G. K., and Puckett, A. E.: Equivalence of the Spanwise Lift Distribution to the Spanwise Lift-Influence Function for Slender Wings and Wing Bodies. Jour. Aero. Sci. (Readers' Forum), vol. 18, no. 7, July 1951, pp. 503-504.

6. Mirels, Harold: Theoretical Method for Solution of Aerodynamic Forces on Thin Wings in Nonuniform Supersonic Stream With an Application to Tail Surfaces. NACA TN 1736, 1948.

7. Sacks, Alvin H.: Behavior of Vortex System Behind Cruciform Wings. Motions of Fully Rolled-Up Vortices. NACA TN 2605, 1952.

8. Edwards, Samuel Sherman: Experimental and Theoretical Study of Factors Influencing the Longitudinal Stability of an Air-to-Air Missile at a Mach Number of 1.4. NACA RM A51J19, 1952.

9. Rainey, Robert W.: An Investigation of Several Supersonic Missile Configurations Directed Toward Minimizing Center-of-Pressure Travel. NACA RM L52G01, 1952.

10. Grigsby, Carl E.: Tests at Mach Number 1.62 of a Series of Missile Configurations Having Tandem Cruciform Lifting Surfaces. NACA RM L51J15, 1952.

11. Allen, H. Julian, and Perkins, Edward W.: Characteristics of Flow Over Inclined Bodies of Revolution. NACA RM A50L07, 1951.

12. Hatch, John E., Jr., and Hargrave, L. Keith: Effects of Reynolds Number on the Aerodynamic Characteristics of a Delta Wing at a Mach Number of 2.41. NACA RM L51H06, 1951.

[redacted]

13. Nielsen, Jack N., and Kaattari, George E.: Method for Estimating Lift Interference of Wing-Body Combinations at Supersonic Speeds. NACA RM A51J04, 1951.

14. Kaattari, George E., Nielsen, Jack N., and Pitts, William C.: Method for Estimating Pitching-Moment Interference of Wing-Body Combinations at Supersonic Speed. NACA RM A52B06, 1952.

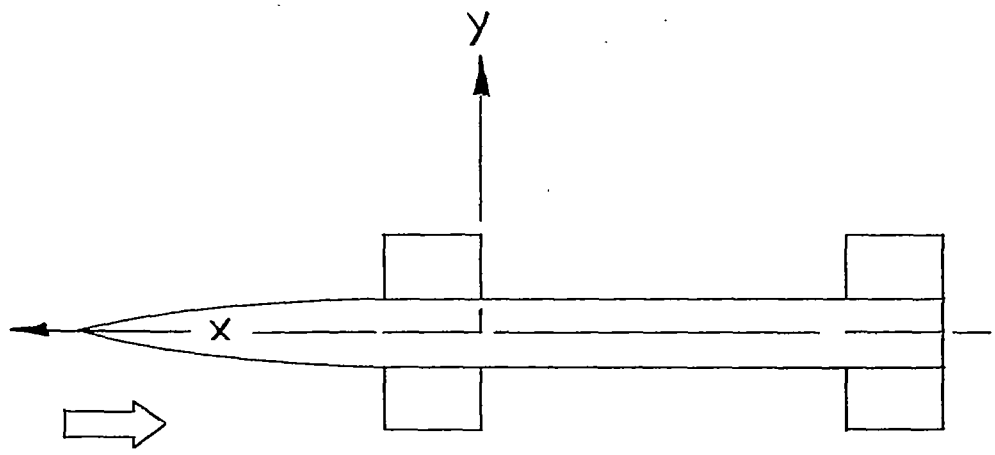

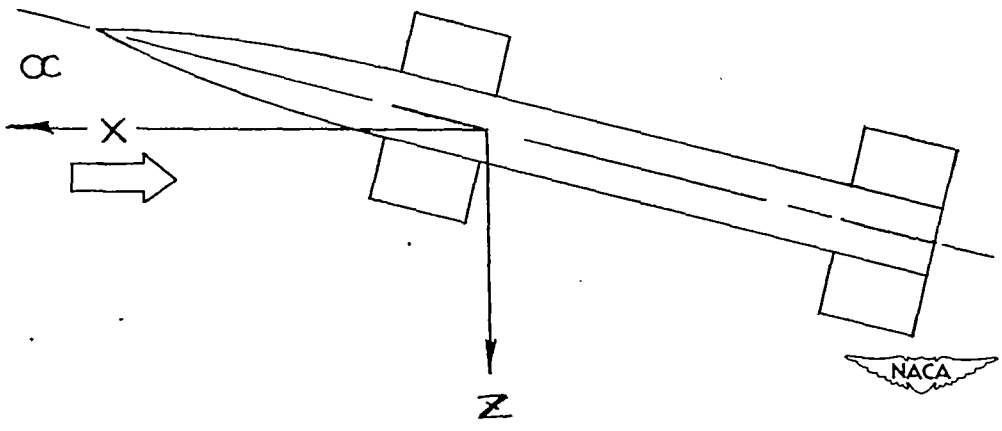

Figure 1.- Sketch of coordinate system.

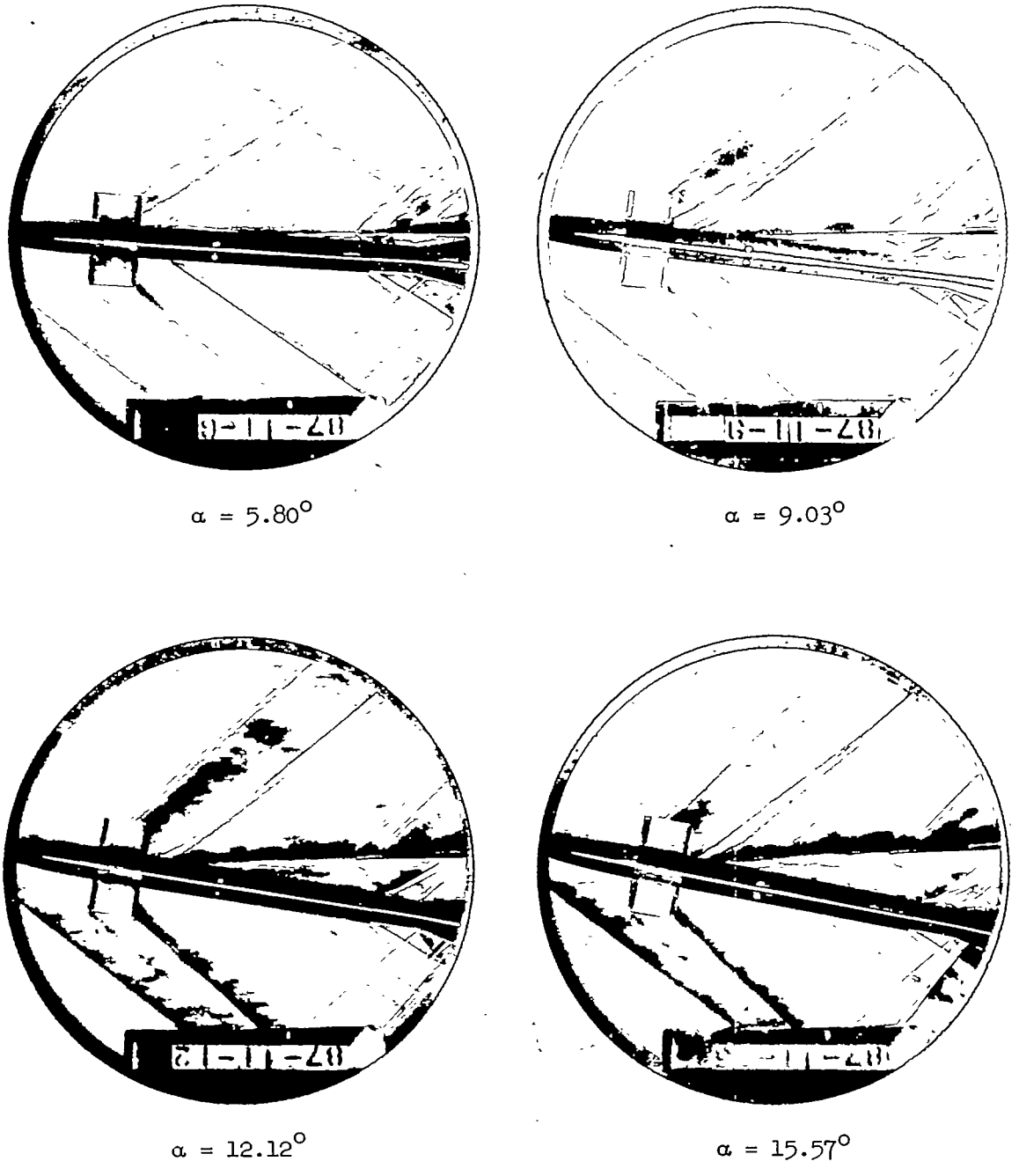

$\alpha = 5.80^\circ$ $\alpha = 9.03^\circ$

$\alpha = 12.12^\circ$ $\alpha = 15.57^\circ$

(a) $BW_{2F}{}^{0}$.

NACA L-75172

Figure 2.- Representative schlieren pictures illustrating vortex patterns behind inline and interdigitated configurations and pitot-tube survey technique.

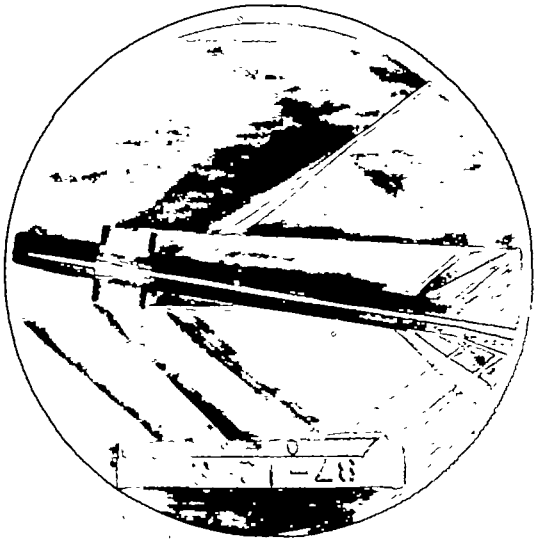

$\alpha = 9.03^\circ$

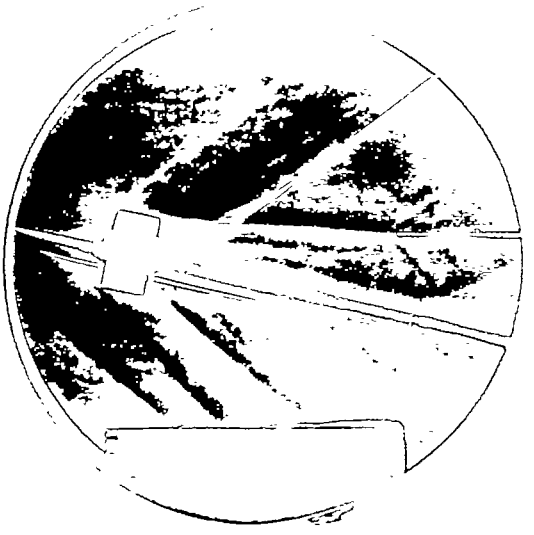

$\alpha = 12.12^\circ$

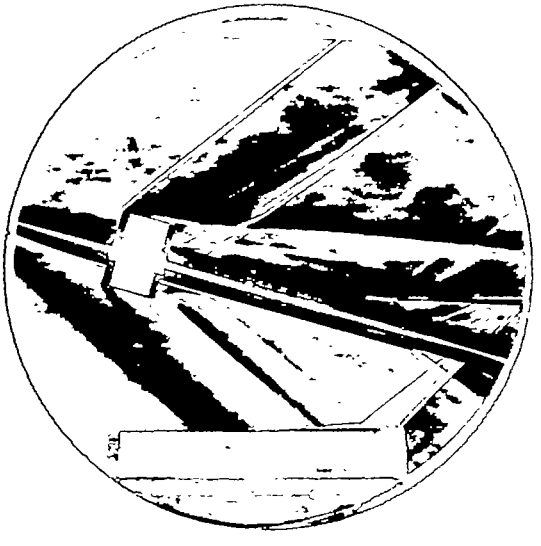

$\alpha = 15.57^\circ$

(b) BW_{2F}^{45}.

NACA
L-75173

Figure 2.- Continued.

[redacted]

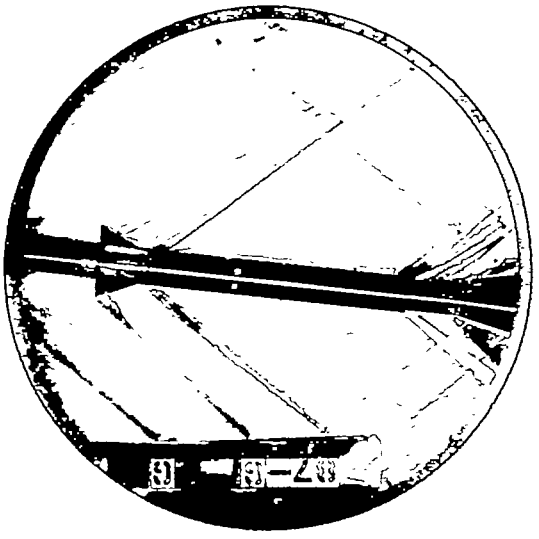

$\alpha = 5.80°$

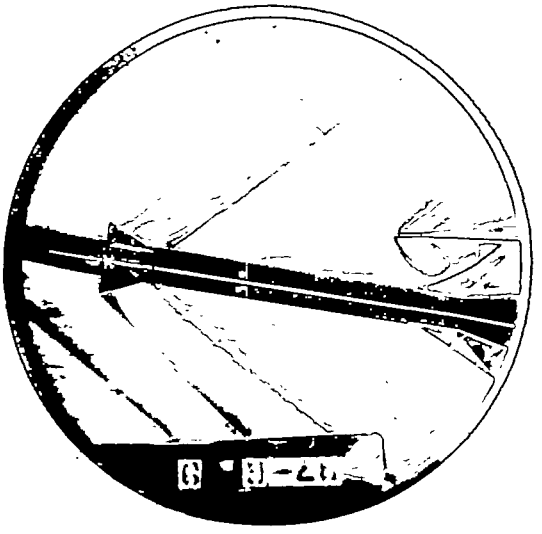

$\alpha = 9.03°$

$\alpha = 12.12°$

(c) $BW_{4F}45$.

NACA
L-75174

Figure 2.- Continued.

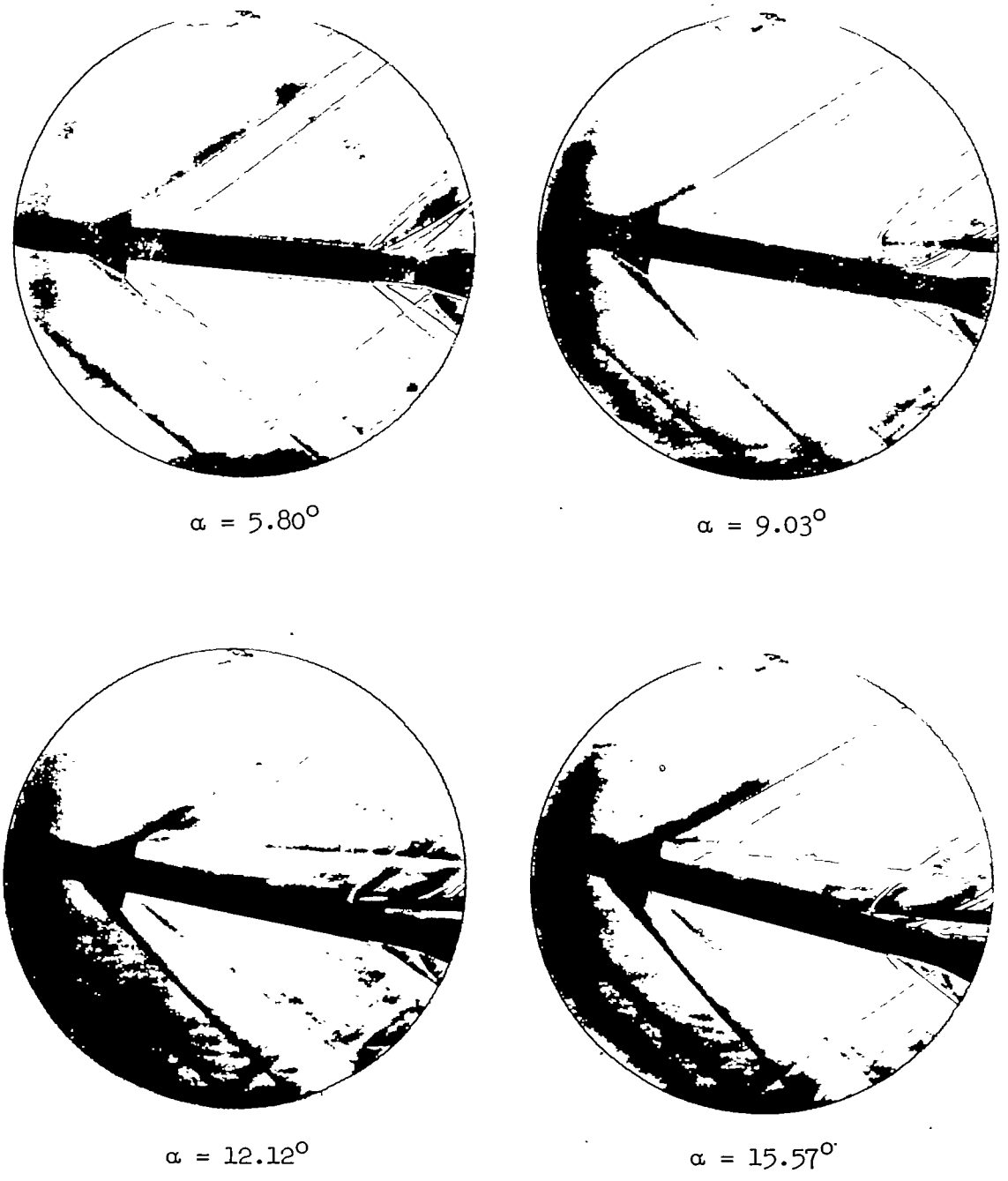

(d) $BW_{5F}^{.45}$.

NACA L-75175

Figure 2.- Concluded.

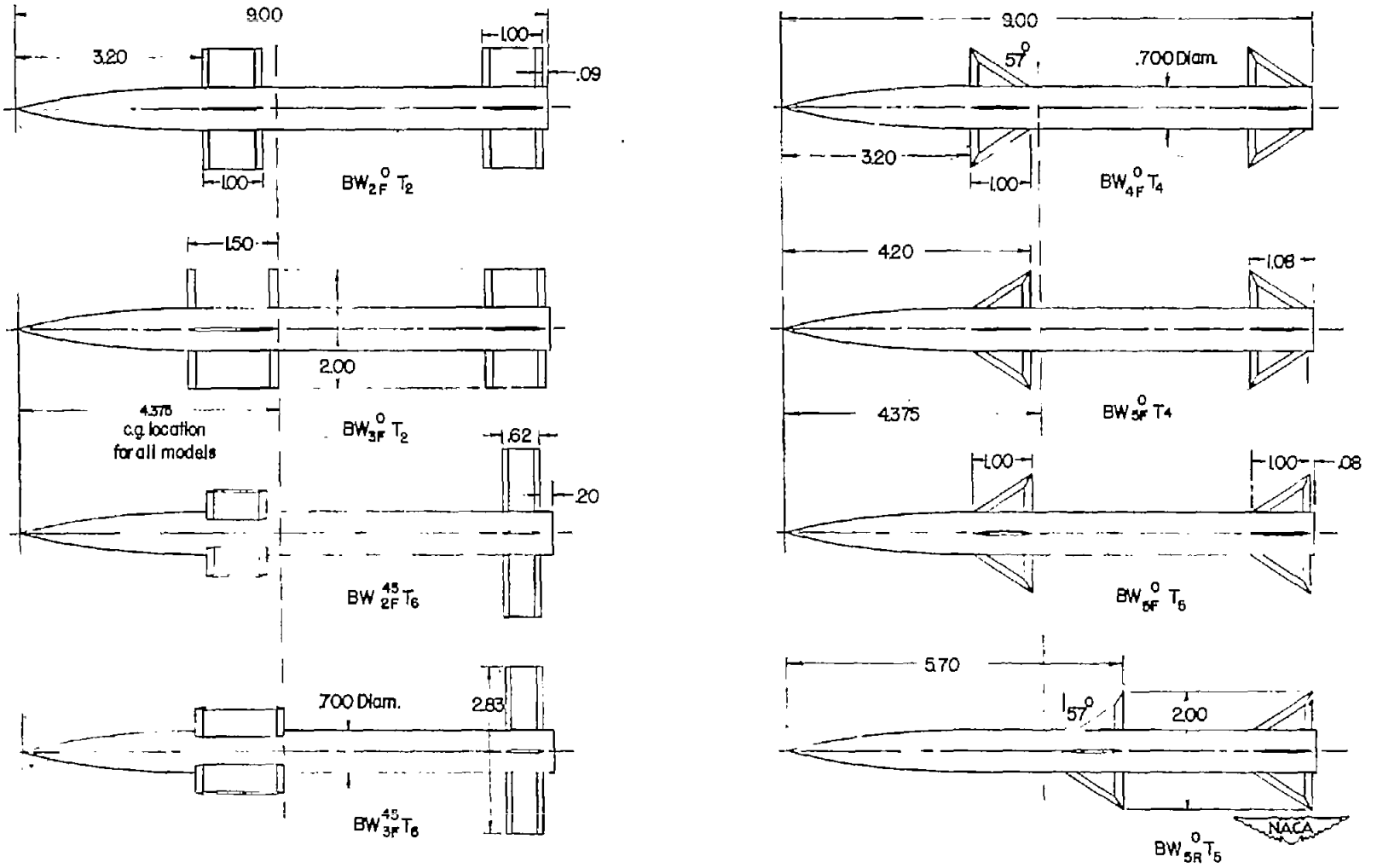

Figure 3.- Detail of models.

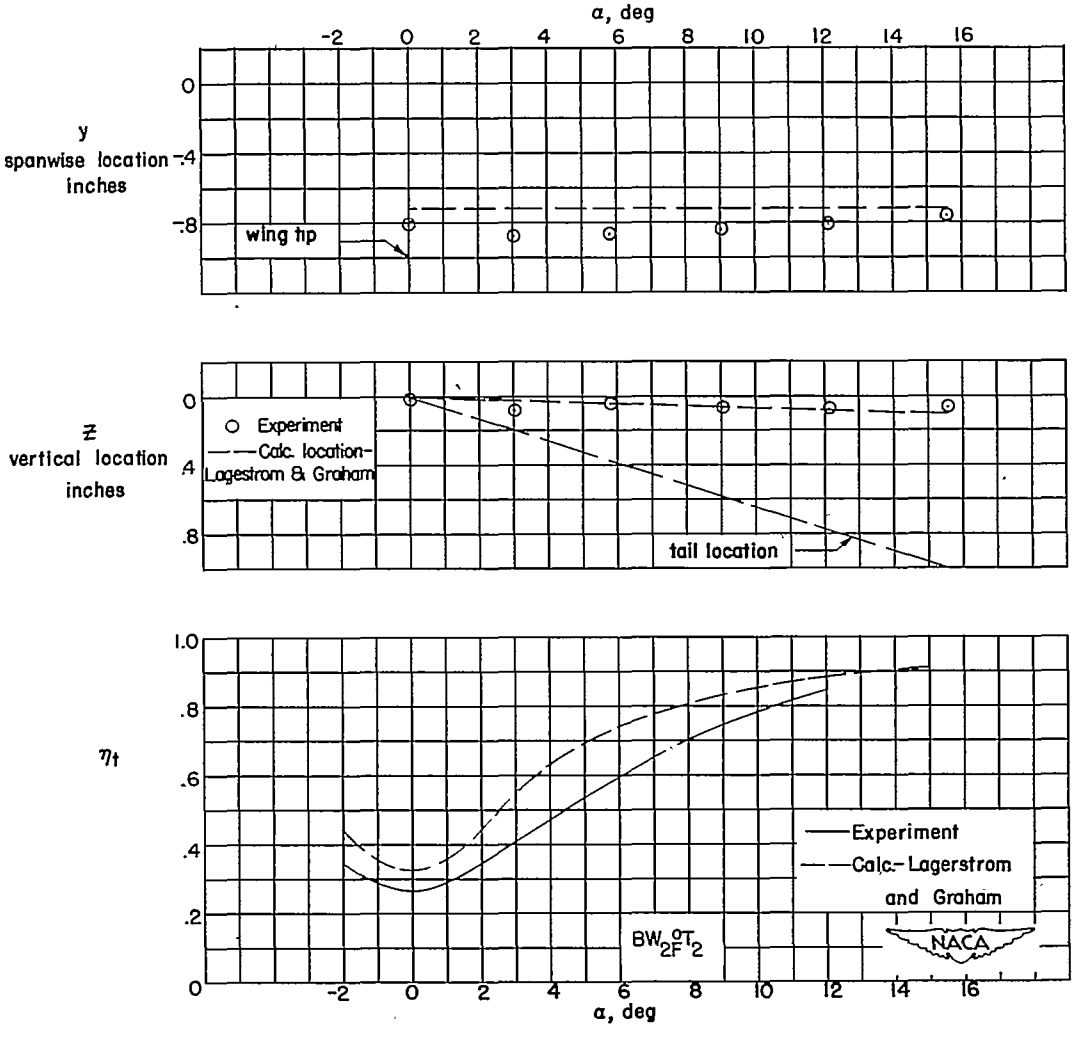

Figure 4.- Measured and assumed vortex locations and tail efficiency parameter variation with angle of attack for configuration $BW_{2F}{}^{O}T_2$.

[redacted]

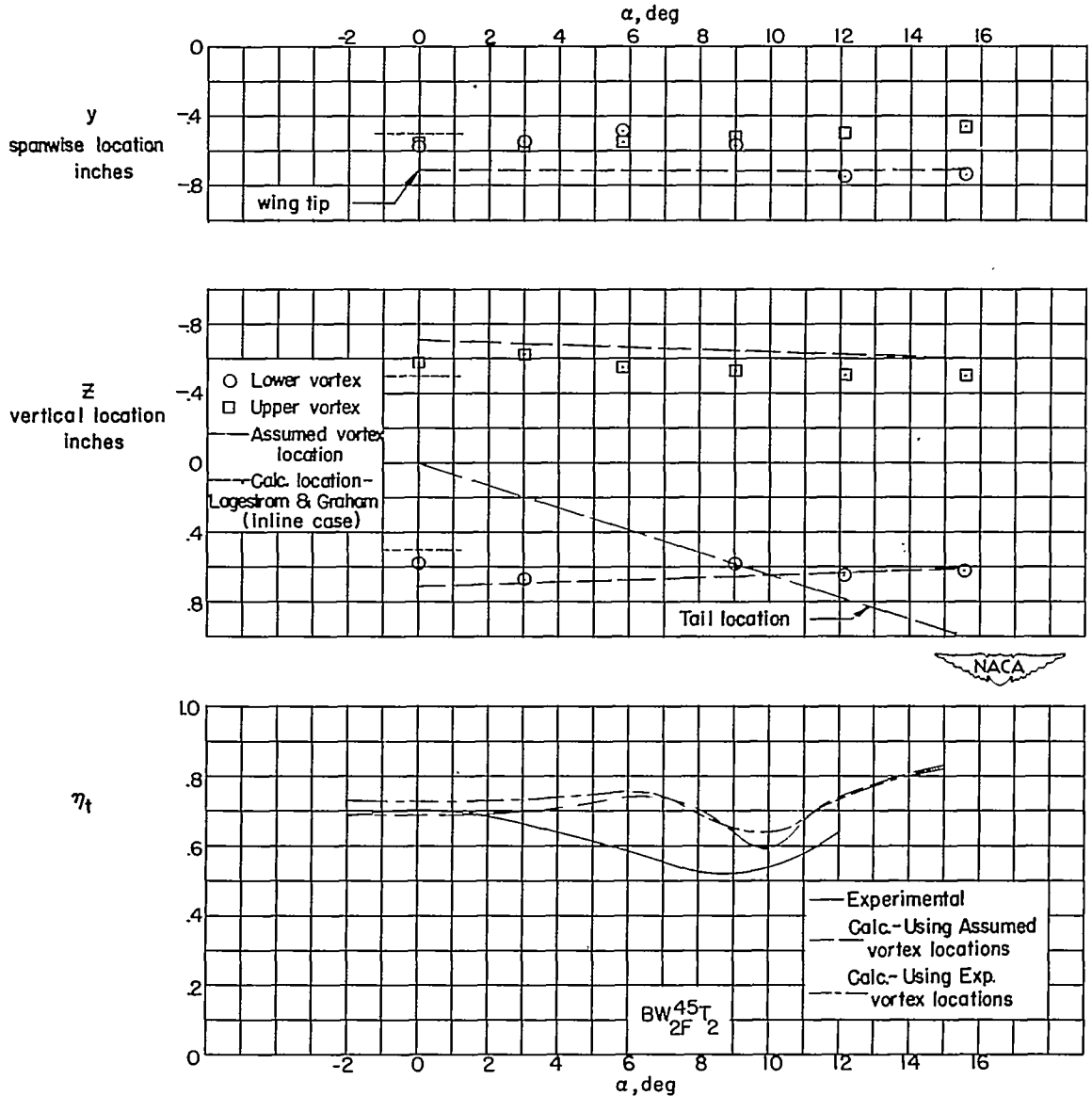

Figure 5.- Measured and assumed vortex locations and tail efficiency parameter variation with angle of attack for configuration $BW_{2F}^{45}T_2$.

[redacted]

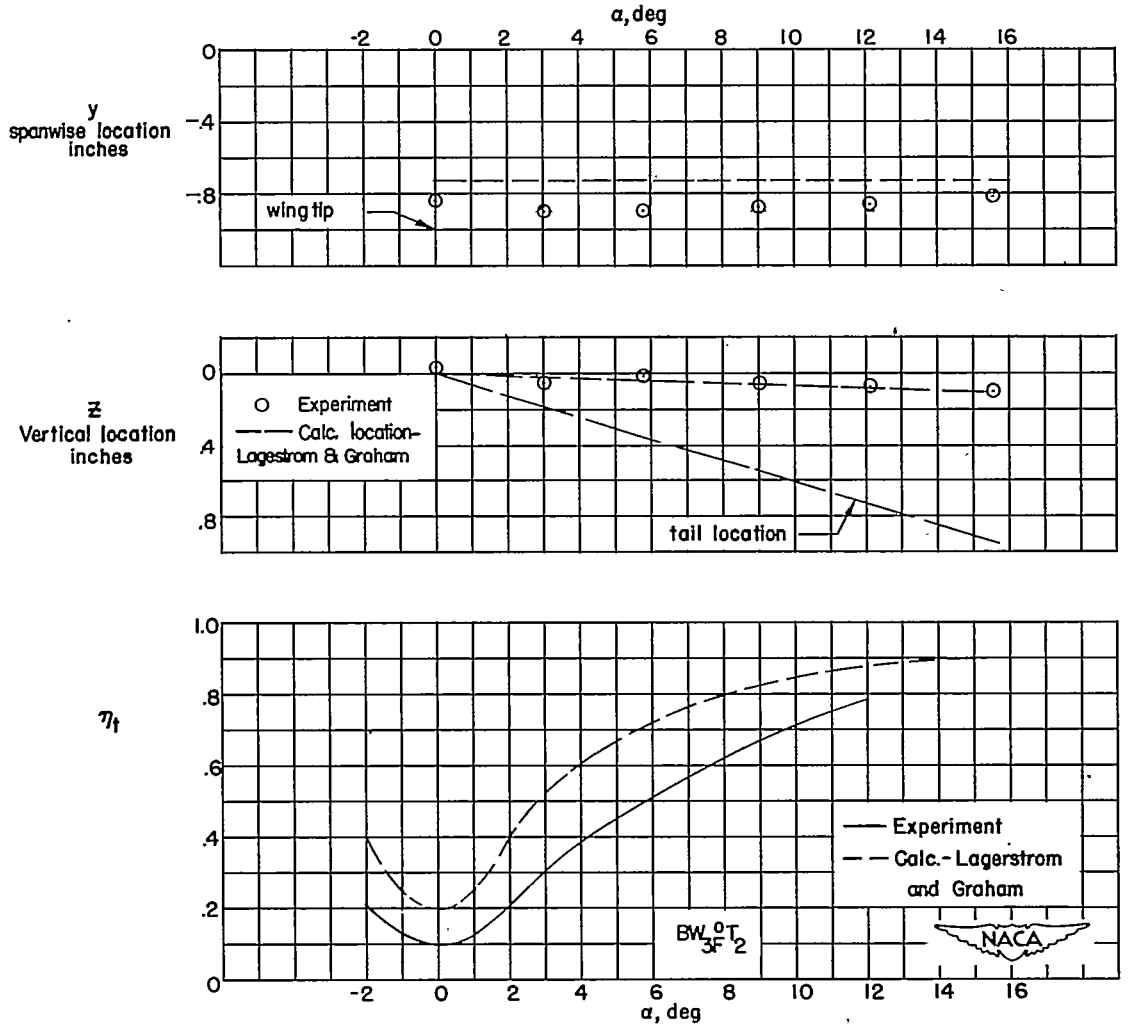

Figure 6.- Measured and assumed vortex locations and tail efficiency parameter variation with angle of attack for configuration $BW_{3F}{}^{0}T_{2}$.

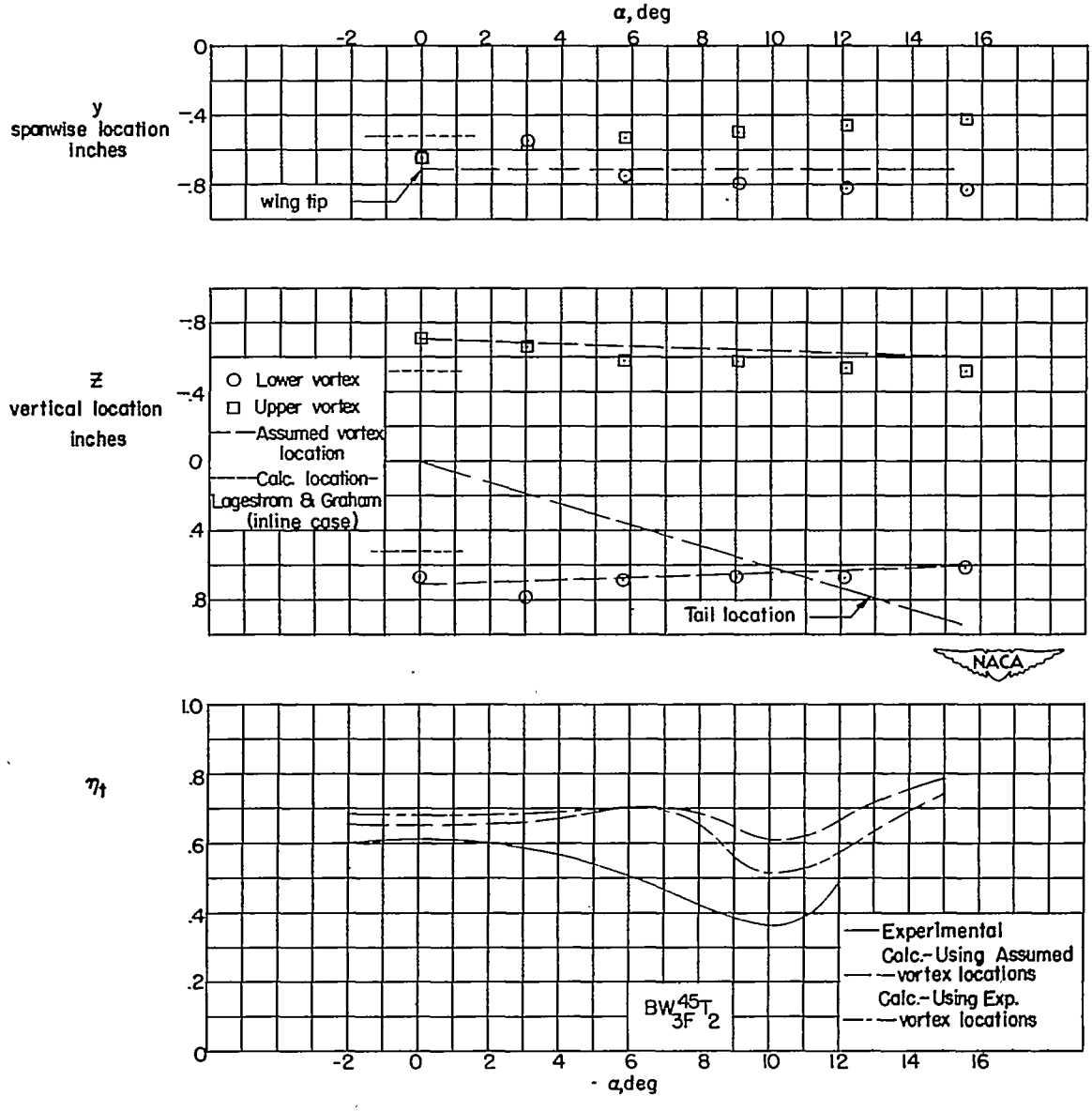

Figure 7.- Measured and assumed vortex locations and tail efficiency parameter variation with angle of attack for configuration $BW_{3F}^{45}T_2$.

[redacted]

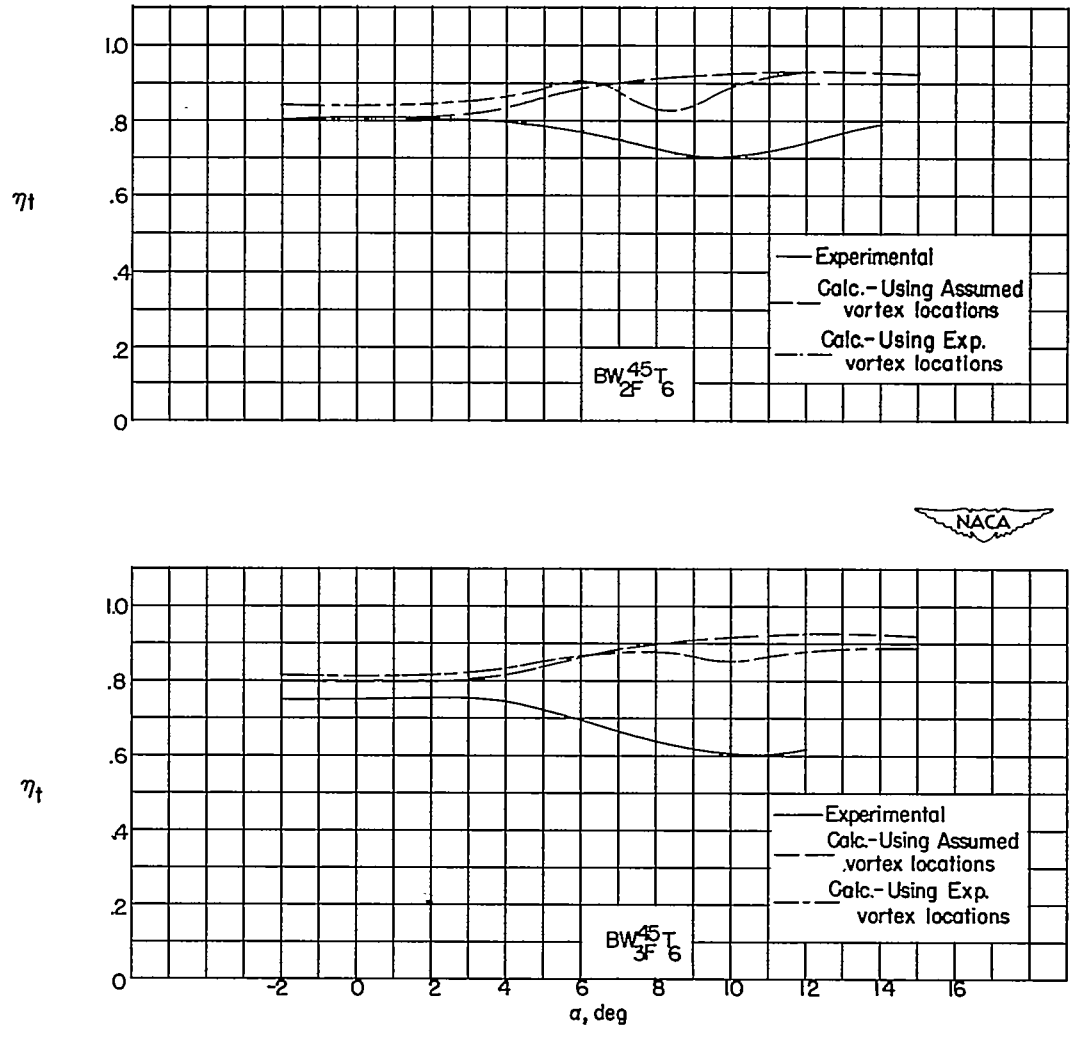

Figure 8.- Tail efficiency parameter variation with angle of attack for configurations $BW_{2F}^{45}T_6$ and $BW_{3F}^{45}T_6$.

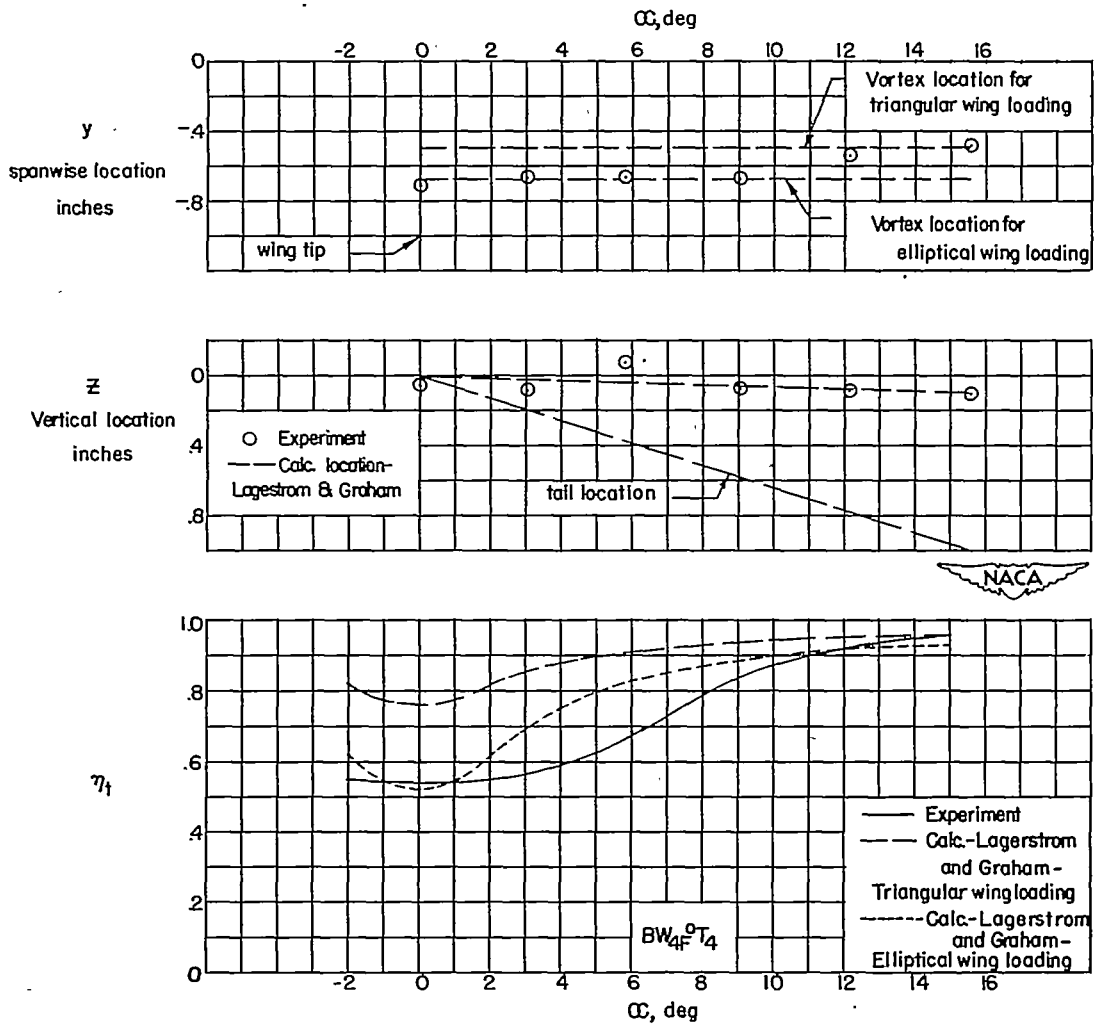

Figure 9.- Measured and assumed vortex locations and tail efficiency parameter variation with angle of attack for configuration $BW_{4F}{}^{O}T_4$.

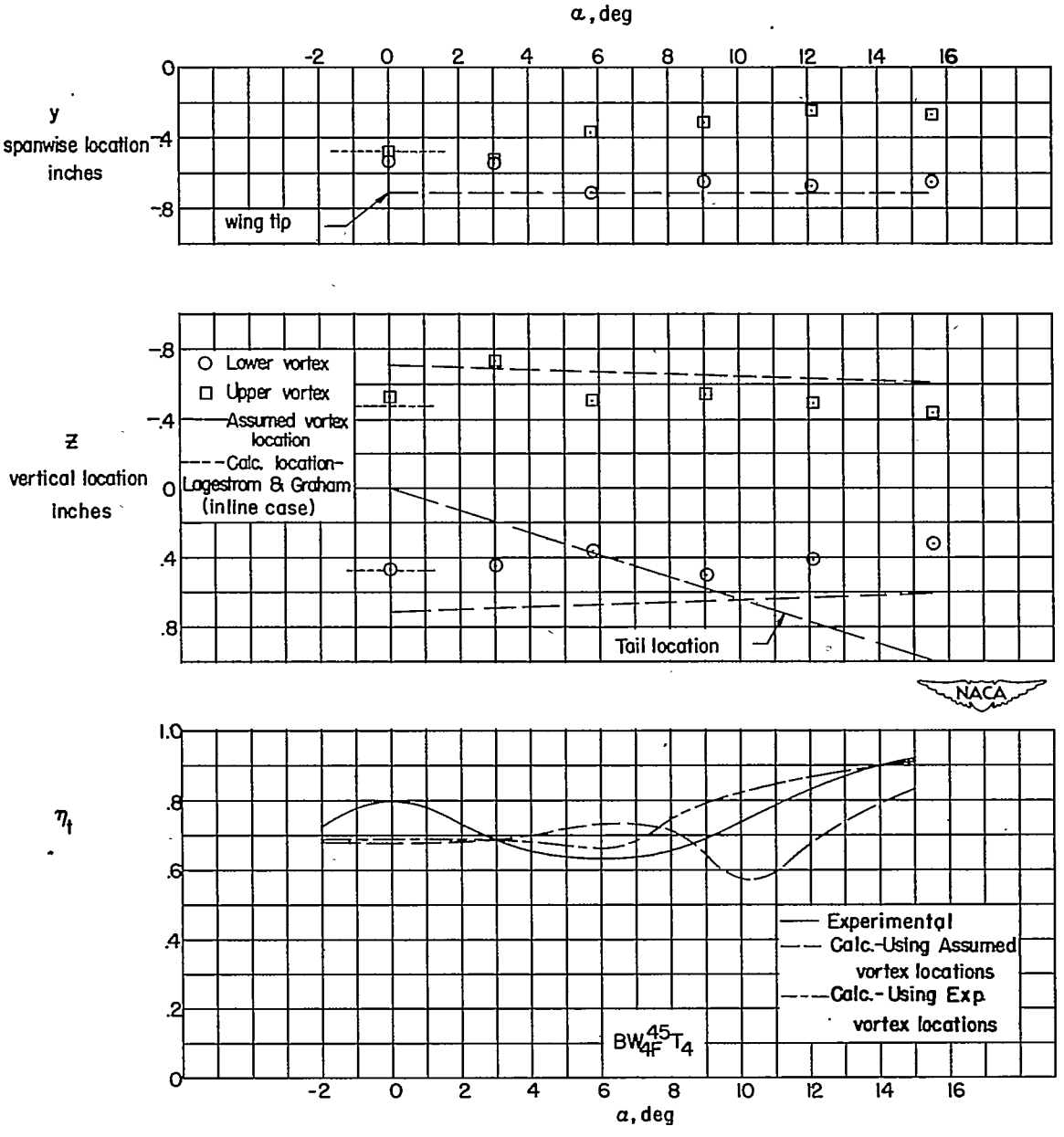

Figure 10.- Measured and assumed vortex locations and tail efficiency parameter variation with angle of attack for configuration $BW_{4F}^{45}T_4$.

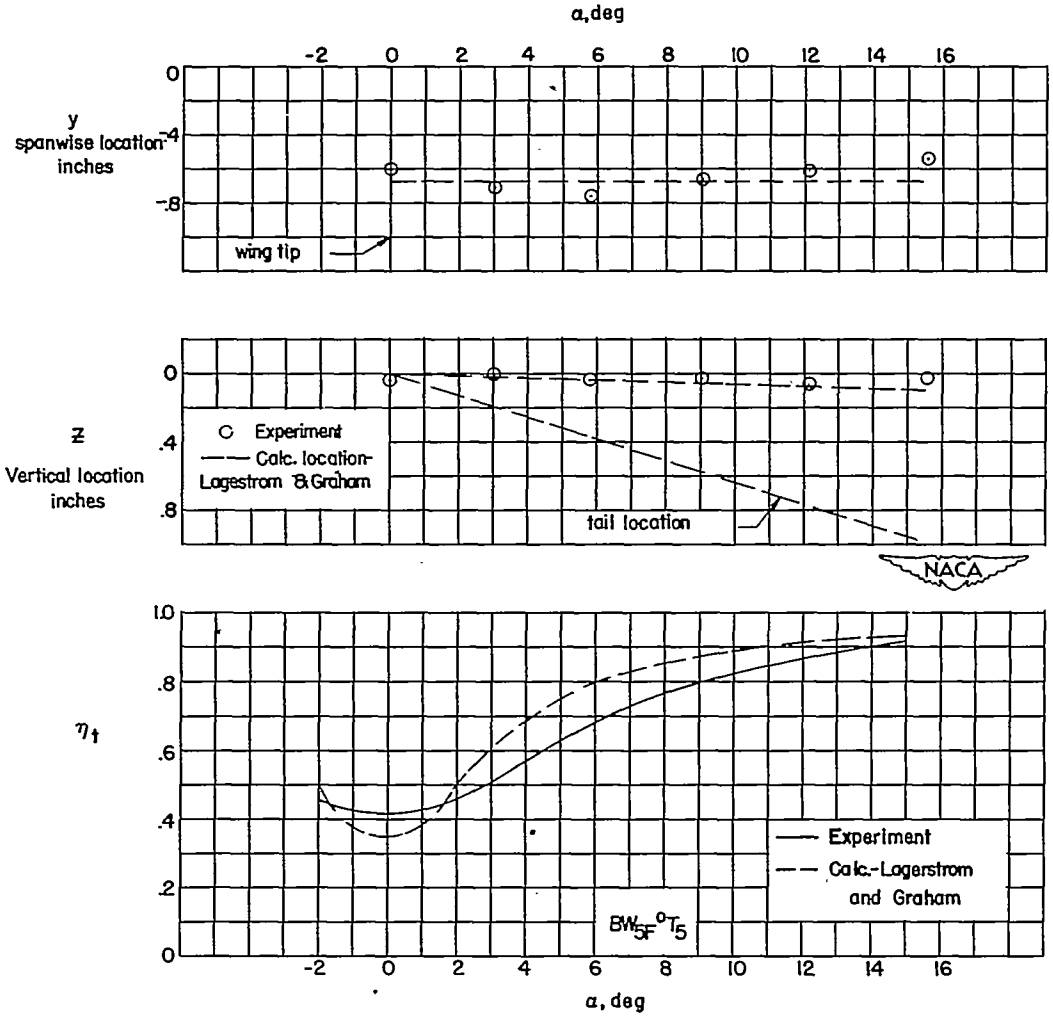

Figure 11.- Measured and assumed vortex locations and tail efficiency parameter variation with angle of attack for configuration $BW_{5F}{}^{O}T_5$.

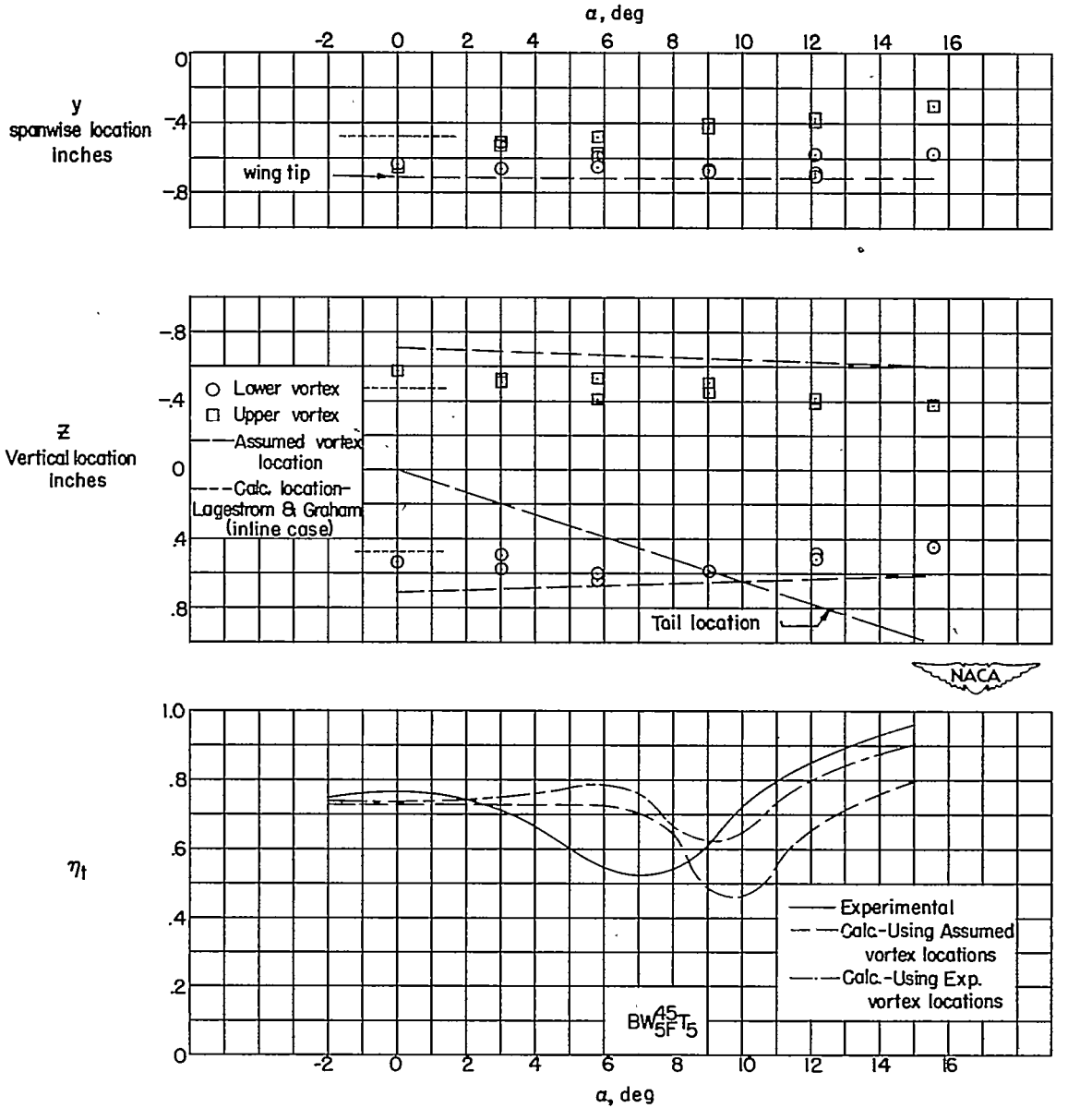

Figure 12.- Measured and assumed vortex locations and tail efficiency parameter variation with angle of attack for configuration $BW_{5F}^{45}T_5$.

[redacted]

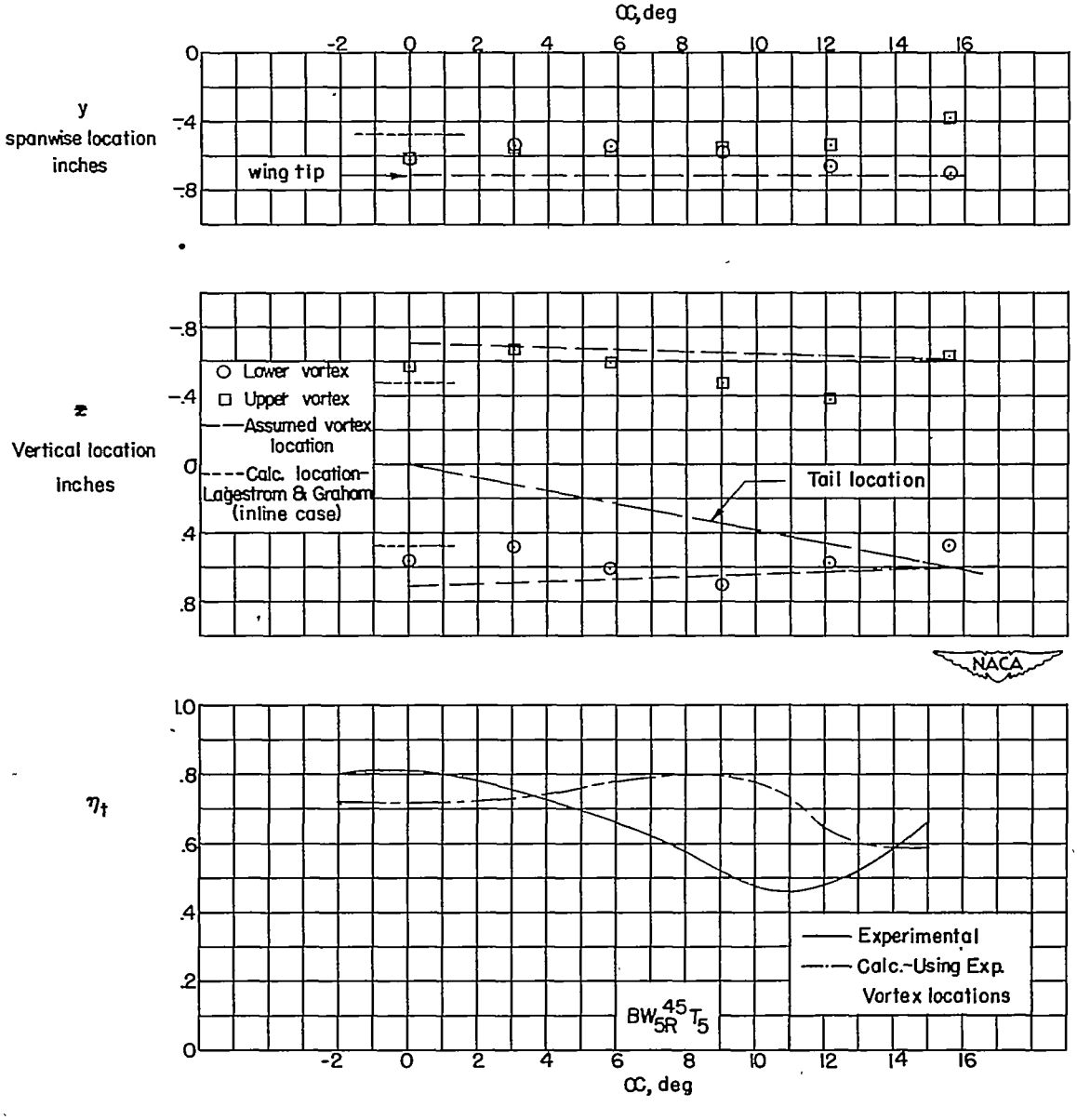

Figure 13.- Measured and assumed vortex locations and tail efficiency parameter variation with angle of attack for configuration $BW_{5R}^{45}T_5$.

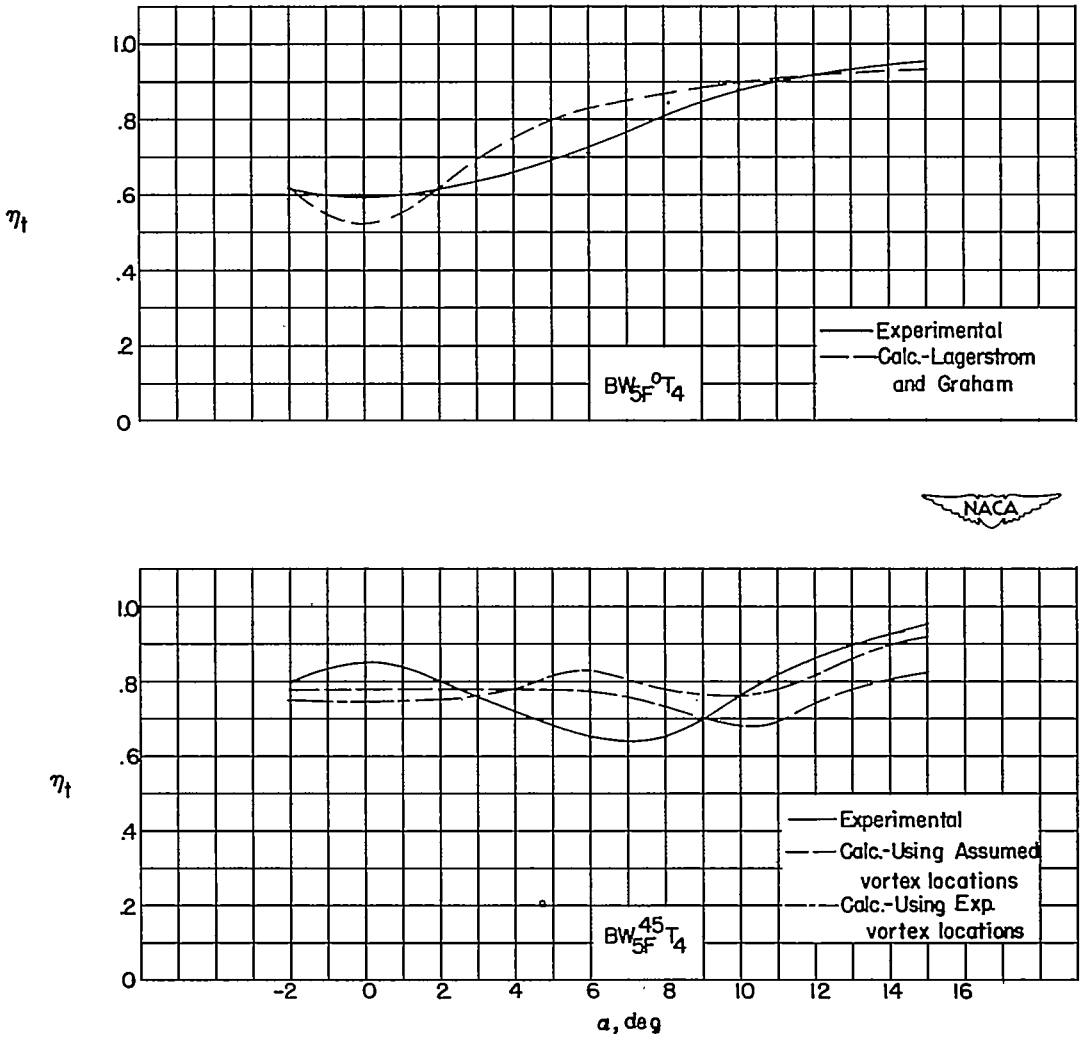

Figure 14.- Tail efficiency parameter variation with angle of attack for configurations $BW_{5F}{}^{0}T_4$ and $BW_{5F}{}^{45}T_4$.

[redacted]

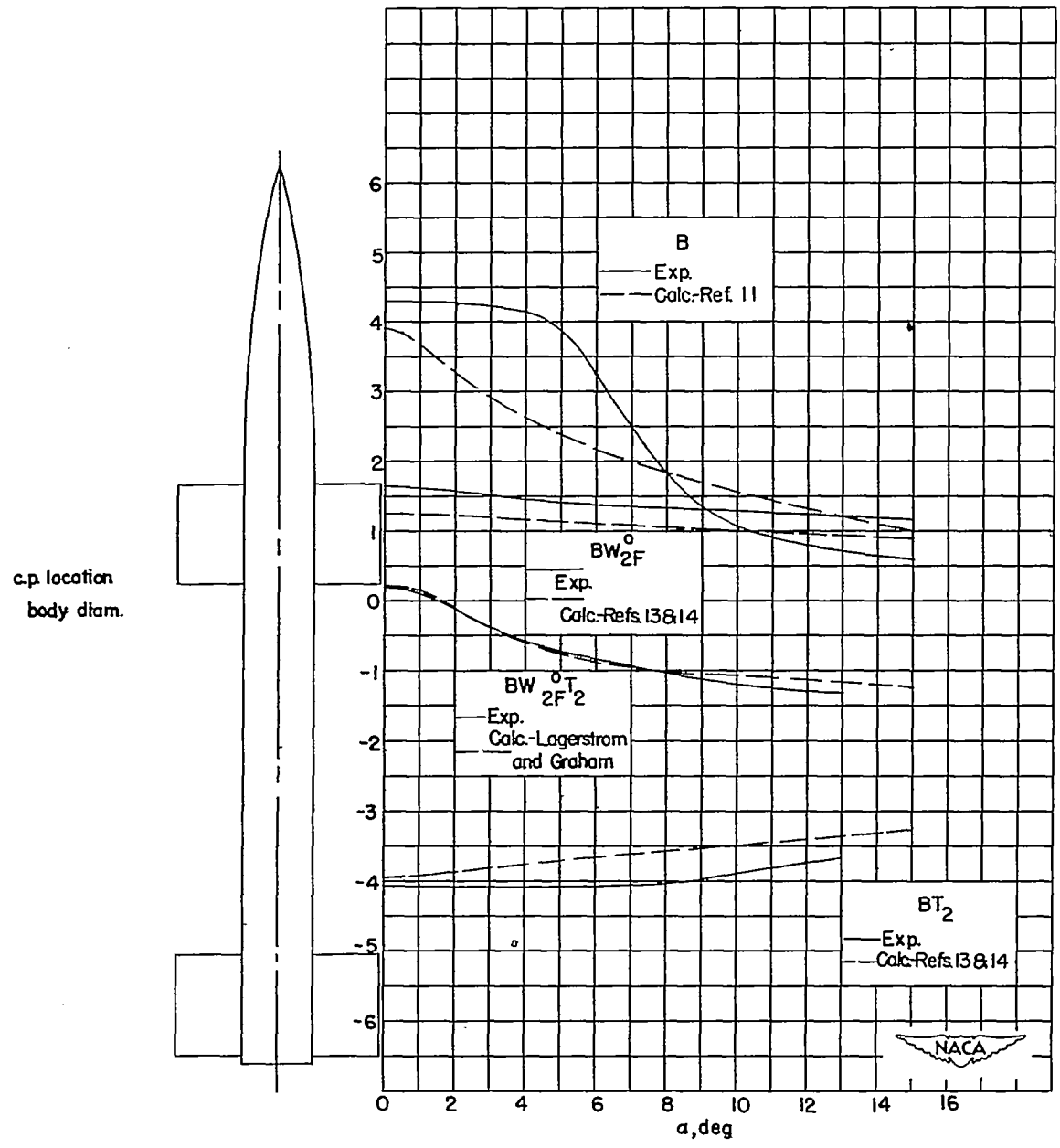

(a) $BW_{2F}{}^{o}T_2$.

Figure 15.- Comparison of experimental and calculated center-of-pressure locations for B, BW, BT, and BWT configurations.

[redacted]

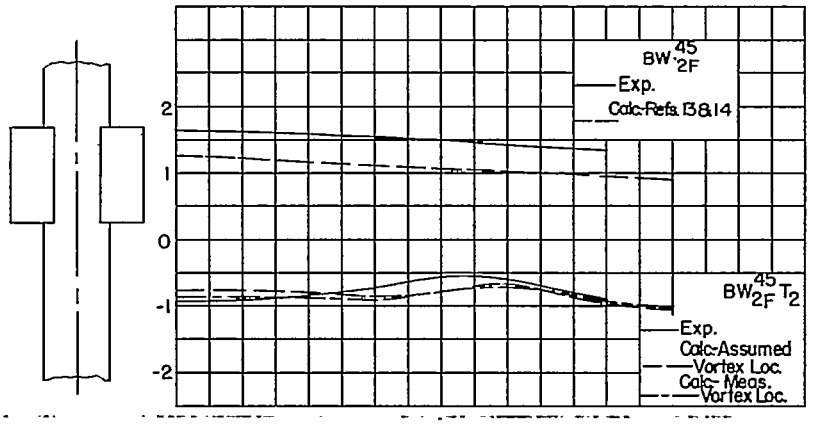

(b) $BW_{2F}^{45}T_2$.

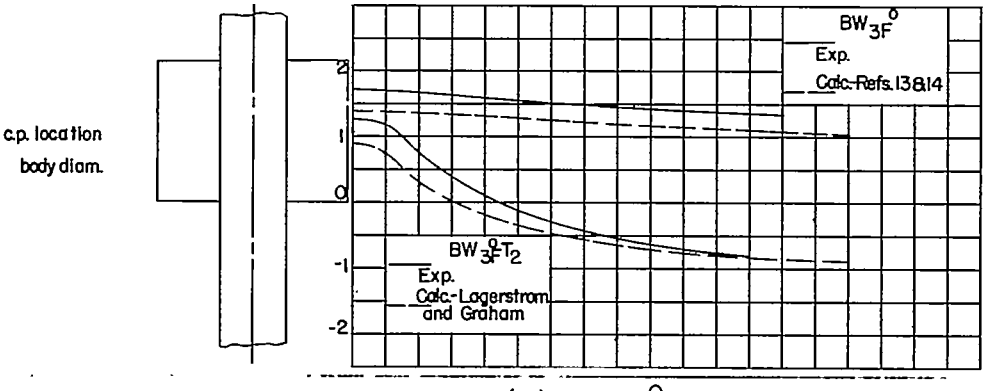

(c) $BW_{3F}^{0}T_2$.

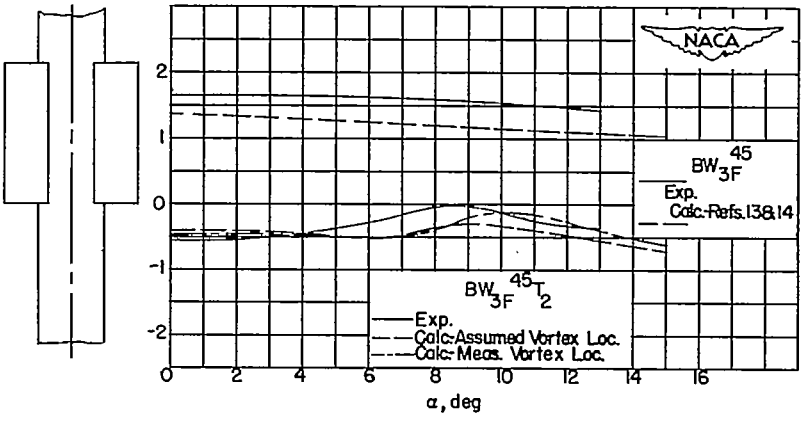

(d) $BW_{3F}^{45}T_2$.

Figure 15.- Continued.

[redacted]

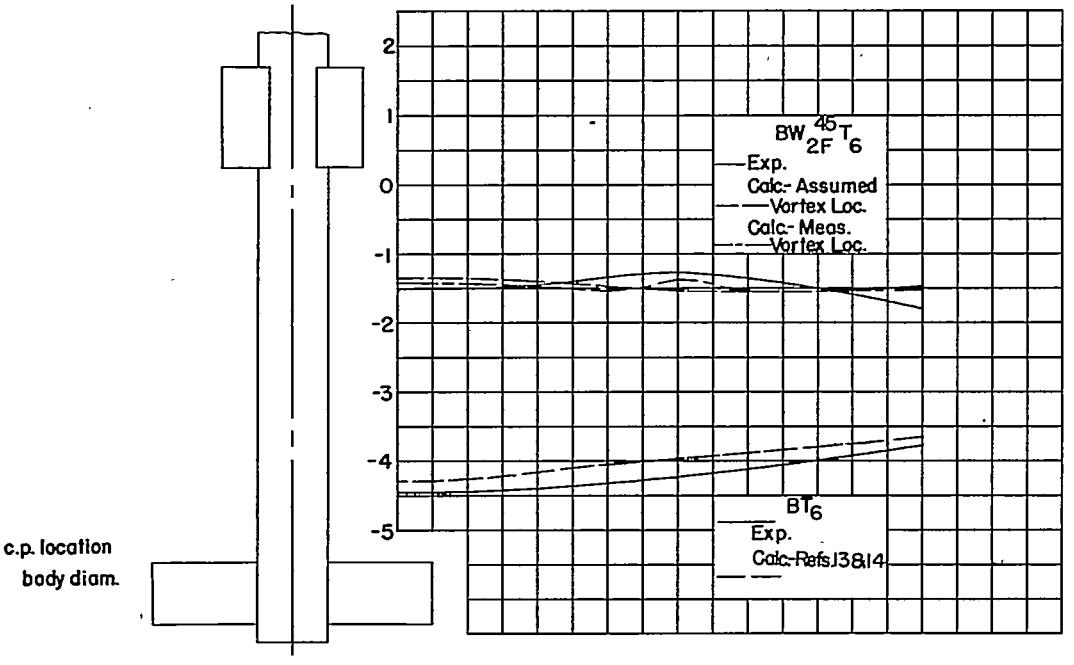

(e) $BW_{2F}{}^{45}T_6$.

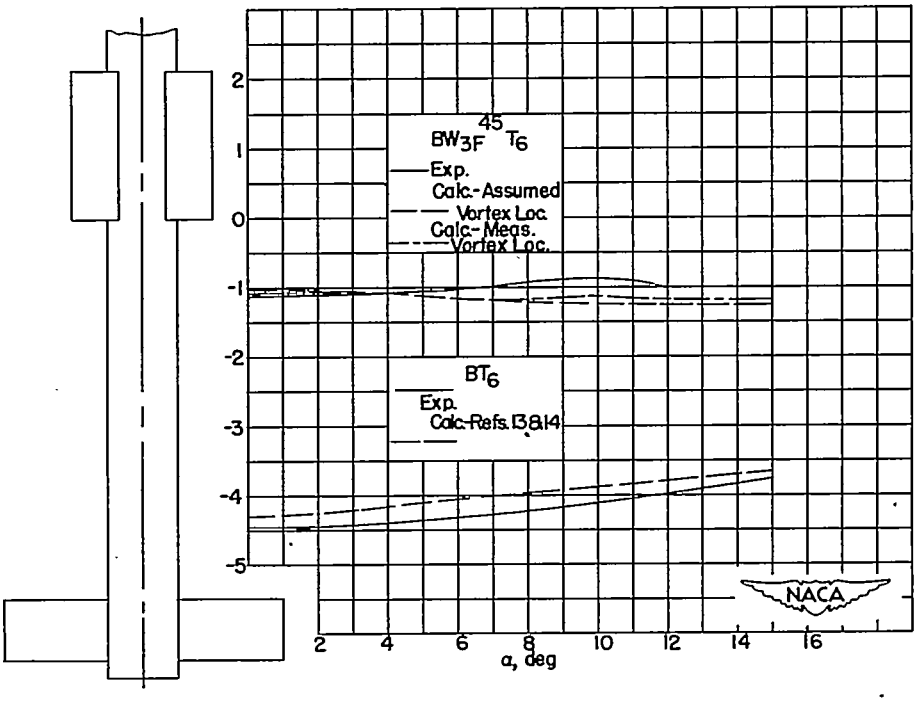

(f) $BW_{3F}{}^{45}T_6$.

Figure 15.- Continued.

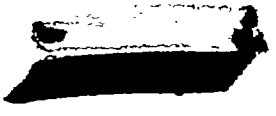

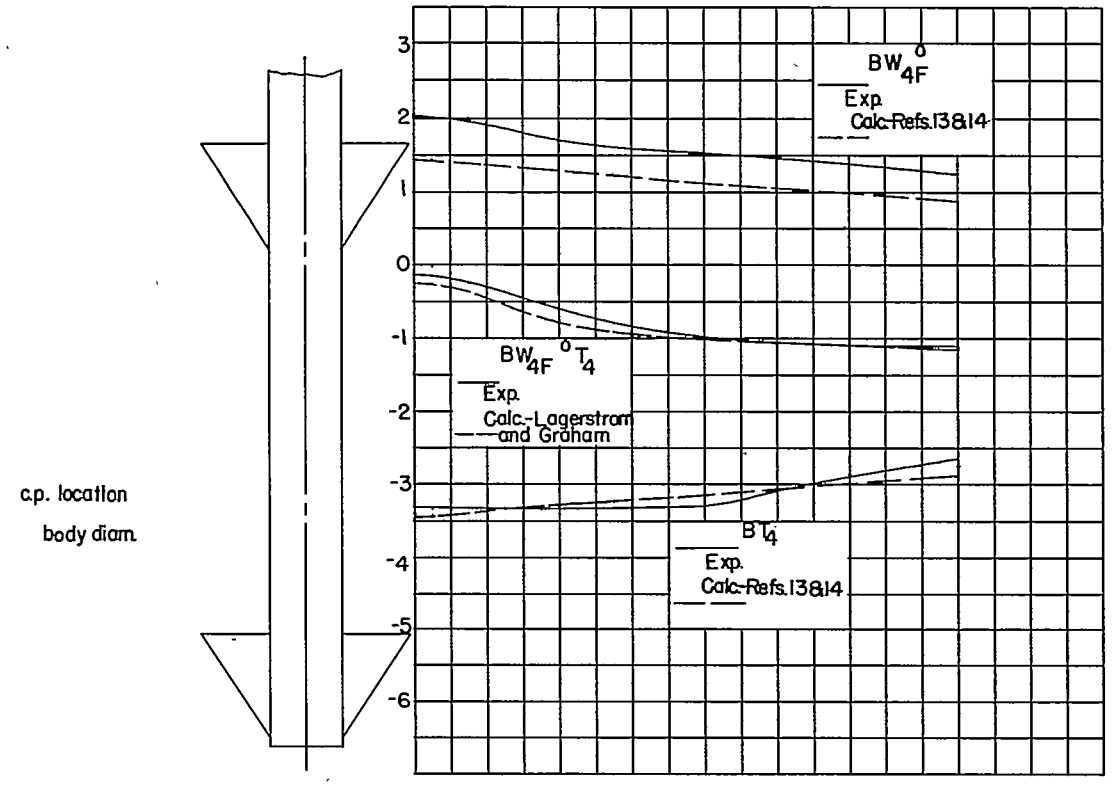

(g) $BW_{4F}{}^{0}T_4$.

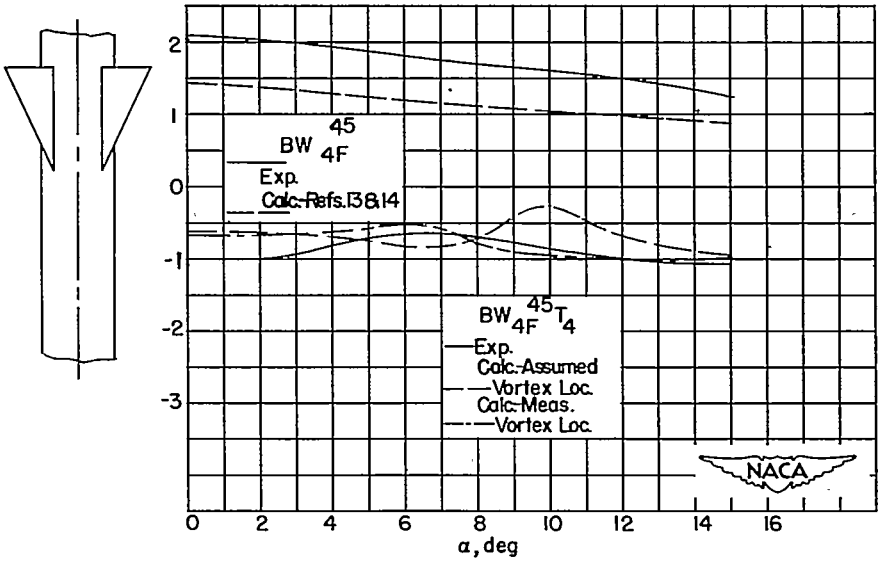

(h) $BW_{4F}{}^{45}T_4$.

Figure 15.- Continued.

[redacted]

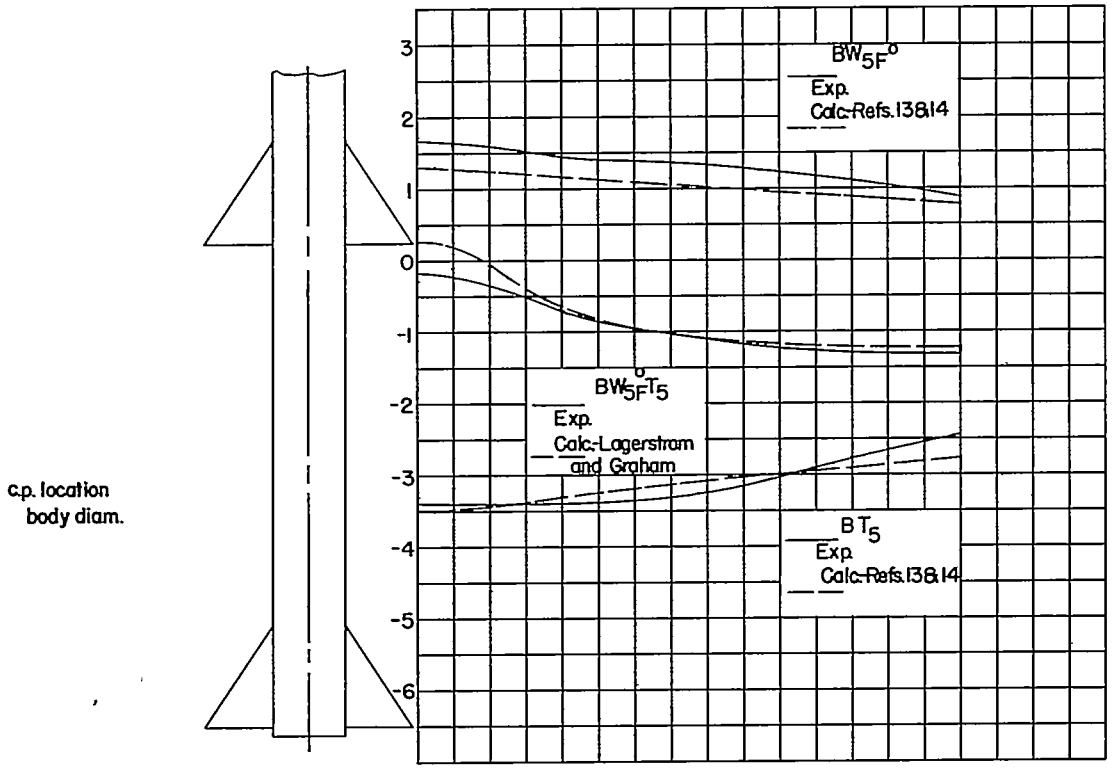

(i) $BW_{5F}{}^{0}T_5$.

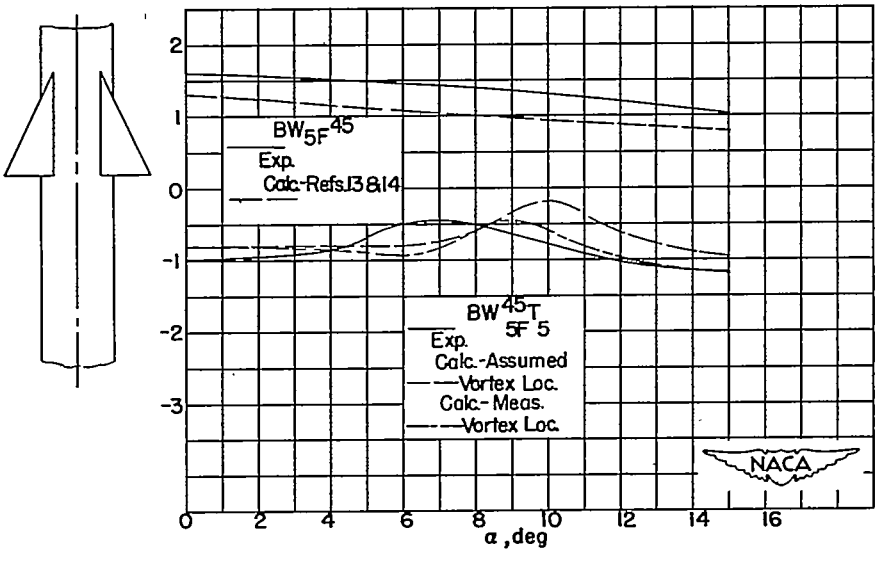

(j) $BW_{5F}{}^{45}T_5$.

Figure 15.- Continued.

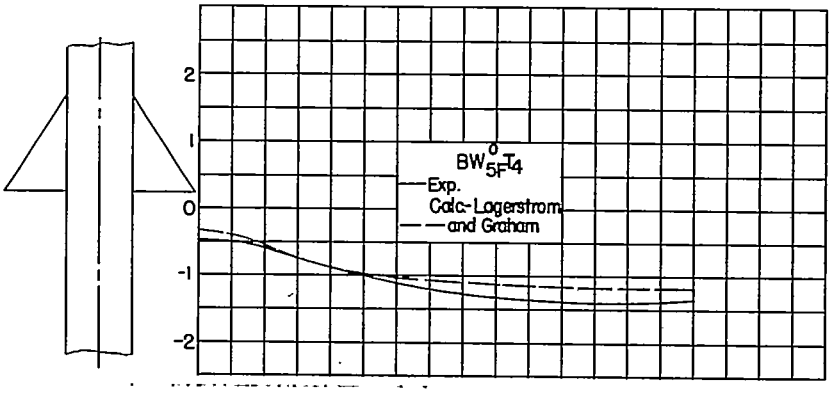

(k) $BW_{5F}{}^{0}T_4$.

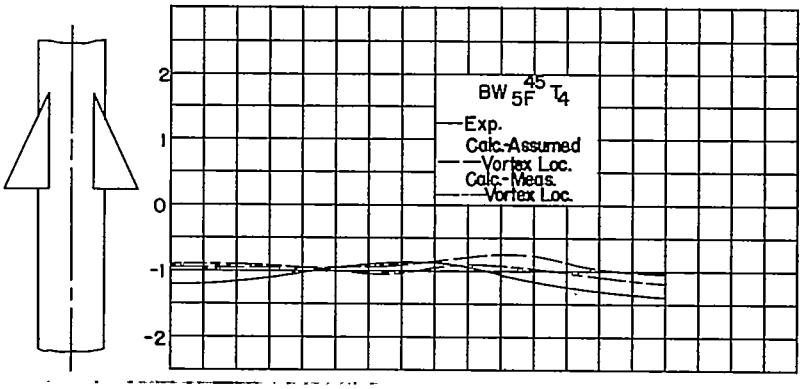

(l) $BW_{5F}{}^{45}T_4$.

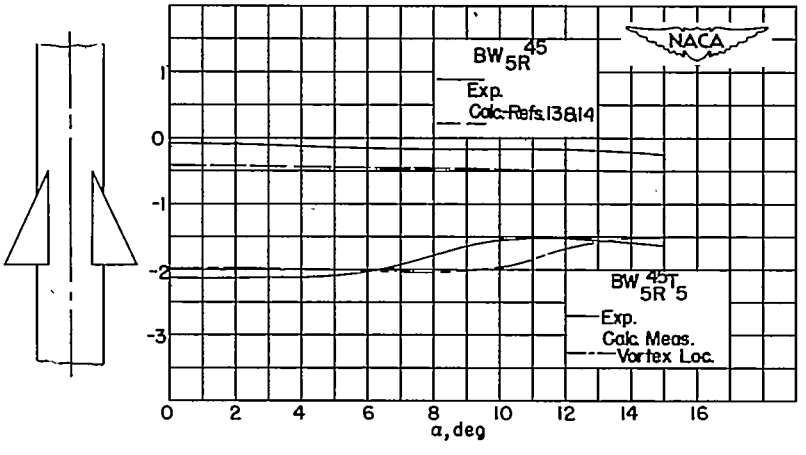

(m) $BW_{5R}{}^{45}T_5$.

Figure 15.- Concluded.

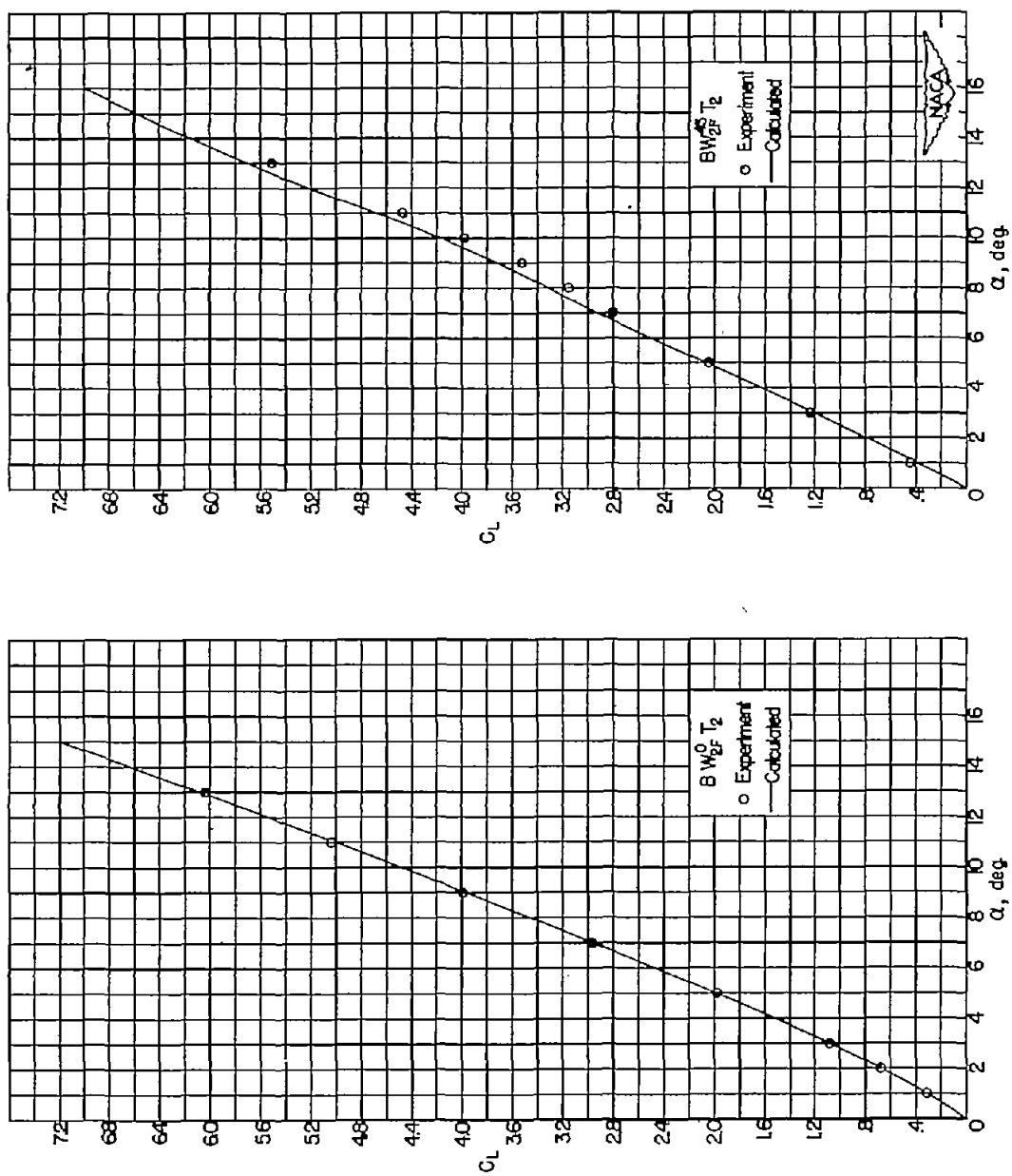

Figure 16.- Representative comparison of experimental and calculated lift coefficients.

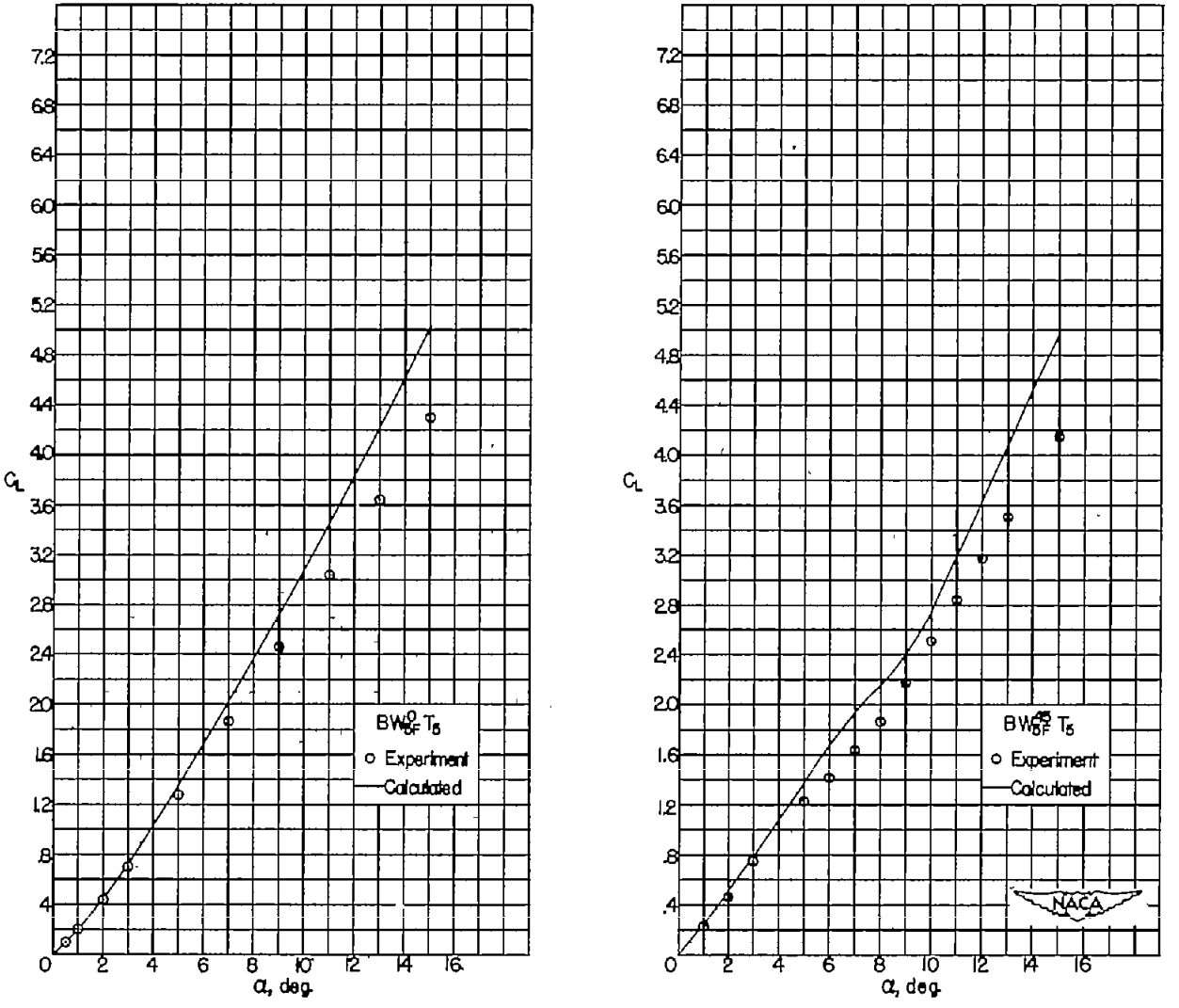

Figure 16.- Concluded.